Journal Pre-proof

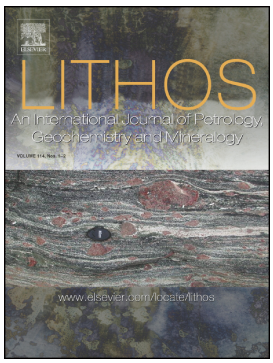

Proto-Tethys magmatic evolution along northern Gondwana: Insights from Late Silurian–Middle Devonian A-type magmatism, East Kunlun Orogen, Northern Tibetan Plateau, China

Jiajie Chen, Lebing Fu, Junhao Wei, David Selby, Daohan Zhang, Hongzhi Zhou, Xu Zhao, Yan Liu

PII: S0024-4937(19)30464-5

DOI: https://doi.org/10.1016/j.lithos.2019.105304

Reference: LITHOS 105304

To appear in: *LITHOS*

Received date: 18 August 2019

Revised date: 25 October 2019

Accepted date: 26 November 2019

Please cite this article as: J. Chen, L. Fu, J. Wei, et al., Proto-Tethys magmatic evolution along northern Gondwana: Insights from Late Silurian–Middle Devonian A-type magmatism, East Kunlun Orogen, Northern Tibetan Plateau, China, *LITHOS*(2019), https://doi.org/10.1016/j.lithos.2019.105304

This is a PDF file of an article that has undergone enhancements after acceptance, such as the addition of a cover page and metadata, and formatting for readability, but it is not yet the definitive version of record. This version will undergo additional copyediting, typesetting and review before it is published in its final form, but we are providing this version to give early visibility of the article. Please note that, during the production process, errors may be discovered which could affect the content, and all legal disclaimers that apply to the journal pertain.

© 2019 Published by Elsevier.

Journal Pre-proof

Proto-Tethys magmatic evolution along northern Gondwana: Insights from Late Silurian–Middle Devonian A-type magmatism, East Kunlun Orogen, Northern Tibetan Plateau, China

Jiajie Chen[a,b,c], Lebing Fu[b,d], Junhao Wei[b], David Selby[c], Daohan Zhang[b], Hongzhi Zhou[b], Xu Zhao[b], Yan Liu[b]

[a] *State Key Laboratory of Nuclear Resources and Environment, School of Earth Sciences, East China University of Technology, Nanchang, 330013, China*

[b] *Faculty of Earth Resources, China University of Geosciences, Wuhan 430074, China*

[c] *Department of Earth Sciences, University of Durham, Durham DH1 3LE, UK*

[d] *Centre for Exploration Targeting, ARC Centre of Excellence for Core to Crust Fluid Systems, University of Western Australia, 35 Stirling Highway, Crawley, WA 6009, Australia*

Corresponding author

Junhao Wei

Faculty of Earth Resources, China University of Geosciences,

Lumo Road No. 388, Hongshan District, Wuhan 430074,

Hubei Province, China.

E-mail: junhaow@163.com

Journal Pre-proof

Tel: +86-13437179812.

Journal Pre-proof

Abstract:

The East Kunlun Orogen records the geological evolutions of the Neoproterozoic – Early Paleozoic Proto-Tethyan Ocean and Late Paleozoic–Mesozoic Paleo-Tethys Ocean along northern Gondwana. However, the late-stage evolution of the Proto-Tethyan Ocean and the configuration of peri-Gondwana microcontinents during the Silurian – Devonian is under debate. Here we report new geochronological and geochemical data of A-type granites from the western Wulonggou and the eastern Gouli areas in the East Kunlun Orogen to deepen our understanding of these problems. Zircon LA-ICP-MS U-Pb data reveal that the Danshuigou monzogranite and Shensitian syenogranite from the western Wulonggou area were emplaced simultaneously at 418 ± 3 Ma, while the Niantang syenogranite from the eastern Gouli area was emplaced at 403 ± 2 Ma. All these rocks display high-K calcic-alkalic to shoshonitic and metaluminous to slight peraluminous signatures, with relatively low CaO, Al_2O_3, MgO and Sr, and high FeO_t/MgO, Ga/Al, Zr, and Nb, indicating their A-type affinity. Their moderate whole-rock εNd(t) (-5.3 – -0.6) and zircon εHf(t) (-6.3 – 6.4) are different from those of depleted mantle and old basement rocks, but similar to those of the Ordovician–Silurian granitoids in the East Kunlun Orogen. These chemical signatures, together with the anhydrous, low-pressure and high-temperature characteristics of the magmas, indicate that partial melting of the Ordovician–Silurian granitoids generated these A-type granites. Regionally, these A-type granites and previously reported A-type granites in the East Kunlun Orogen compose a Late Silurian – Middle Devonian A-type granite belt. This belt, together with the regionally coeval molasse

Journal Pre-proof

formation and mafic-ultramafic rocks, indicate a post-collisional extensional regime for the East Kunlun Orogen during the Late Silurian – Middle Devonian. Given that extensive contemporaneous post-collision-related magmatic rocks have also been revealed in the neighboring West Kunlun, Altyn, Qilian and Qinling blocks/terranes, we contend that the Neoproterozoic – Early Paleozoic Proto-Tethyan Ocean that separated these blocks/terranes from Gondwana had closed by the Late Silurian – Middle Devonian, which]resulted in the re-welding of the above blocks/terranes to northern Gondwana or Gondwana-derived microcontinents.

Keywords: A-type granite; post-collision; Proto-Tethys; East Kunlun Orogen; Gondwana

Journal Pre-proof

1. Introduction

The Proto-Tethyan Ocean was an ancient ocean located along northern Gondwana during the Paleozoic (Raumer and Stampfli, 2008; Li et al., 2018) and its geology is mainly recorded in the Central Orogenic Belt of China. Several microcontinental blocks, such as the Kunlun, Altyn, Qaidam, Qilian and Northern Qinling, were involved in the evolution of this ancient ocean (Fig. 1A; Li et al., 2018 and references therein). Although, it is accepted that the Proto-Tethyan Ocean formed during the break-up of the supercontinent Rodinia since the Neoproterozoic (Li et al., 2018 and references therein), the timings and the processes of the amalgamation of different microcontinents (blocks/terranes) are debated (Song et al., 2014; Xiong, 2014; Liu et al., 2016; Li et al., 2018). For example, both ~462 Ma (Xiong, 2014) and ~440 Ma (Song et al., 2014) have been proposed for the timing of the amalgamation of the Qaidam and Qilian blocks; both 500 Ma (Liu et al., 2016) and post-380 Ma (Li et al., 2018) has been taken as the closure timing of the Shangdan Ocean (a branch of Proto-Tethyan Ocean) which separate the Southern Qinling from Northern Qinling. These ambiguities obscure the reconstruction of the ocean-continent configuration along northern Gondwana.

The East Kunlun Orogen (EKO), which has an Archean–Proterozoic basement, is one of the microcontinental blocks involved in the evolution of the Proto-Tethyan Ocean (Wang et al., 2007; Li et al., 2018) and present day is located in the northern Qinghai-Tibetan Plateau (Fig. 1A). The EKO represents the connection between the Proto-Tethys and Paleo-Tethys domain (Fig. 1A) and hosts abundant geological records regarding the

Neoproterozoic–Early Paleozoic and Late Paleozoic–Cenozoic two-stage orogenesis, which correspond to the evolutions of the Proto-Tethyan Ocean (referred to as the Central Kunlun Ocean in the EKO) and Paleo-Tethys Ocean (referred to as the A'nyemaqen Ocean in the EKO), respectively (Mo et al., 2007; Song et al., 2018). During the last decade studies have mainly focused on the predominant Permian-Triassic rocks that are related to the evolution of the Paleo-Tethys Ocean, indicating that this ocean opened during the Carboniferous, subducted during the Permian-Early Triassic and closed in the Late Triassic (e.g., Xiong et al., 2014; Chen et al., 2017). In regard to the evolution of the Proto-Tethyan Ocean, related studies are sparse due to the later superimposed tectono-magmatic events. Thus far, a number of zircon U-Pb ages of Cambrian ophiolites have been reported in the EKO (555–481 Ma; Yang et al., 1996; Li, 2006; Liu et al., 2011b; Wei, 2015), which are similar to the ages from the remnants of the Proto-Tethyan Oceanic crust in the West Kunlun (525–489 Ma; e.g., Zhang et al., 2004; Huang et al., 2014), Qilian (550–496 Ma; Song et al., 2014 and references therein) and Qinling blocks (534–457 Ma; Dong et al., 2011 and references therein), indicating that a part of the Proto-Tethyan Ocean should have opened during the Cambrian. The subduction of the Proto-Tethyan Ocean is evidenced by the Cambrian–Silurian arc-related granitoids (518–436 Ma; Zhang et al., 2010; Liu et al., 2011a; Li et al., 2015; Chen et al., 2016). However, the late-stage evolution of the Proto-Tethyan Ocean is under debate and the dispute is centered around whether this ocean closed during the Silurian–Devonian (Zhang et al., 2014; Song et al., 2018) or inherited by the Paleo-Tethys Ocean through protracted subduction (Zhou et al., 2016; Dong et al., 2018).

Several Silurian–Devonian A-type granites are reported in the EKO, and although sparse, the A-type granites describe an east-west trend (Fig. 1B). Given that A-type granites can reflect extensional environments on a local or regional scale (Eby, 1992; Bonin et al., 1998; Wu et al., 2002), the extensive A-type granites in the EKO offers an ideal opportunity to investigate the late-stage evolution of the Proto-Tethyan Ocean. In this contribution, we focus on A-type granites from the western Wulonggou and eastern Gouli areas in the EKO and present their petrographic, geochronological, major and trace elemental and Sr-Nd-Hf isotopic data to: (1) study the origin of these A-type granites, (2) detect the rock-forming setting and implications for the evolution of the Proto-Tethyan Ocean and (3) discuss the evolution and regional configuration of the microcontinents along northern Gondwana during the Early Paleozoic.

2. Geological setting

The EKO is bounded by the Qaidam Basin to the north, the Qinling Orogen to the east, the Bayan Har-Garze Terrane to the south and the Altyn Tagh Fault in the west (Fig.1A). It is composed of the Northern Qimantag Belt, Northern East Kunlun Terrane and Southern East Kunlun Terrane, which are separated by the Northern East Kunlun Suture zone (Dong et al., 2018; Dong et al., 2019) and Central East Kunlun Suture zone (Fig. 1B; e.g., Meng et al., 2013). The basement rocks exposed in the EKO are intermediate–high-grade metamorphic rocks referred to as the Paleoproterozoic Jinshuikou and Kuhai Group, Mesoproterozoic Xiaomiao Formation and Meso-Neoproterozoic Wanbaogou Group

(Zhang et al., 2005; Wang et al., 2007). Among them, the Jinshuikou Group and Xiaomiao Formation are distributed in the Northern Qimantag belt and the Central East Kunlun Terrain; The Kuhai and Wanbaogou groups are located in the Southern East Kunlun Terrain (Dong et al., 2018). The overlying strata include Paleozoic and Mesozoic sedimentary, low-grade metamorphic and volcanic rocks (e.g., Zhang et al., 2005). Among them, the Ordovician Naij Tal Group, which mainly occur in the Southern East Kunlun Terrane, consists of meta-sandstone, metapelite and meta-volcanic rocks (e.g., Chen et al., 2014). This group is unconformably overlain by the Devonian Maoniushan Formation (400–423 Ma), which is composed of conglomerate, sandstone and continental volcanic rocks (e.g., Lu et al., 2010). Overlying the Maoniushan Formation is the Carboniferous–Permian strata that consist of marine and paralic clastic formations (Xiong et al., 2014). Magmatic rocks are widespread in the EKO and are dominated by granitoids, with minor mafic and ultramafic rocks. The ultramafic rocks mainly compose three regional ophiolite belts, i.e., Northern East Kunlun Suture zone, Central East Kunlun Suture zone and Southern East Kunlun Suture Zone, which pass through the whole EKO from west to east (Fig. 1B). The ophiolites from the Central East Kunlun Suture zone and Southern East Kunlun Suture Zone show age populations that are dominantly Cambrian (522–467 Ma) and Carboniferous (345–332 Ma), corresponding to ridge expansions of the Proto-Tethyan Ocean and Paleo-Tethys Ocean, respectively (Yang et al., 1996; Chen et al., 2001; Liu et al., 2011b; Wei, 2015), with the ophiolite from the Qimantag representing relics of Early Paleozoic back-arc basin (501—486 Ma; Meng et al., 2015; Zheng et al., 2016; Dong et al., 2019).

The predominant granitoids include I-, S- and A-type units, which show two distinct emplacement episodes (470–380 Ma and 260–220 Ma) (Mo et al., 2007; Xiong et al., 2015; Chen et al., 2017) and display time-varying lithology from early calc-alkaline granodiorites to late monzogranites and syenogranites in both episodes (Xiong et al., 2014; Xiong et al., 2015; Chen et al., 2016).

The Wulonggou and Gouli areas are located in the western and eastern part of the EKO, respectively (Fig. 1B). In the Wulonggou area, the principal strata are composed of Proterozoic metamorphic rocks (e.g., gneiss and schist) and the Ordovician Tanjianshan Group low-grade meta-sedimentary and meta-volcanic rocks, which were intruded by the Devonian and Triassic magmatic rocks (Fig. 1C). The Devonian magmatic intrusions include gabbro, syenogranite, porphyritic monzogranite and alkali-feldspar granite (Lu et al., 2013), with the Triassic intrusions mainly comprising plagiogranite, diorite and granodiorite (Fig. 1C; Ding et al., 2014). Similar Proterozoic metamorphic rocks (Wang et al., 2007) and low-grade meta-volcanic and meta-sedimentary rocks (herein referred as Ordovician Naij Tai Group; e.g., Chen et al., 2014) are also exposed in the Gouli area. In addition, Carboniferous-Permian sedimentary rocks are exposed in the northern part of the Gouli area (Fig. 1D). Further, magmatic rocks are dominated by the Ordovician granodiorite (472 Ma; unpublished report) and Devonian syenogranite with minor Triassic monzogranite in this area (Fig. 1D).

3. Petrography and sampling

3.1. Danshuigou monzogranite and Shenshuitan syenogranite from the Wulonggou

area

3.1.1 The Danshuigou monzogranite

The Danshuigou monzogranite that is located in the middle of the Wulonggou area was emplaced into the Proterozoic metamorphic rocks and Ordovician Tanjianshan Group low-grade metamorphic rocks (Fig. 1C). It shows a porphyritic texture (Fig. 2A). The phenocrysts are composed of euhedral to subhedral plagioclase and alkali-feldspar (3–6 mm in length) (Fig. 2B–C). The groundmass is made up of anhedral quartz, subhedral plagioclase, alkali-feldspar, interstitial biotite, minor subhedral hornblende and accessory minerals (Fig. 2B–C). The alkali-feldspar including microcline, perthite and orthoclase composes about 40% of the monzogranite in volume, with volume proportions for plagioclase, quartz and biotite being ~ 35%, 20% and 4%, respectively.

3.1.2. The Shenshuitan syenogranite

The Shenshuitan syenogranite that is situated in the west of the Wulonggou area was emplaced into the Ordovician metamorphic rocks (Fig. 1C). It has a light red color and coarse-grained texture (Fig. 2D). The sizes of the primary minerals are approximately 3–8 mm in length (Fig. 2E–F). This intrusion has same mineral assemblage as the Danshuigou monzogranite and is also composed of euhedral-subhedral alkali-feldspar (40–50 %), plagioclase (25-35 %), anhedral quartz (20–30 %), interstitial biotite (2 %) and hornblende (1 %) with minor accessory minerals. The grain sizes of light-color minerals (alkali-feldspar and plagioclase) are larger than those of dark-color minerals (biotite and hornblende; Fig. 2E–F). The identical mineral compositions between the monzogranite and syenogranite,

together with their close spatial relationship (Fig. 1C) and same rock-forming ages (discussed below), may imply that they were sourced from a same parental magma.

3.2. Niantang syenogranite from the Gouli area

The Niantang syenogranite from the Gouli area was emplaced into the Proterozoic and Ordovician metamorphic rocks and was covered by the Carboniferous–Permian sedimentary rocks (Fig. 1D). The syenogranite displays a light-red color and coarse-grained texture (Fig. 2G) and is composed of perthite (35–40%), microcline (10–15%), plagioclase (10–15%), quartz (30–35%), interstitial biotite (3–5 %), minor hornblende (0.5–1 %) and accessory minerals (Fig. 2H–I).

Sample locations for the Danshuigou monzogranite, Shenshuitan syenogranite, and Niantang syenogranite are illustrated in Fig. 1C and Fig. 1D.

4. Analytical methods

Fresh samples selected for whole-rock geochemistry analyses were crushed into 200-mesh powders. Handpicked zircons were prepared for laser ablation inductively coupled plasma mass spectrometry (LA-ICP-MS) U-Pb isotope analyses and multi-collector LA-ICP-MS Hf isotope analyses. Major elements of all samples were analyzed using X-ray fluorescence (XRF) spectrometry at the Australian Laboratory Services' (ALS) Chemex (Guangzhou) Co. Ltd with analytical precision better than 5 %. Whole-rock trace elements and Sr-Nd isotopes, and zircon U-Pb-Hf isotopes of samples from the Wulonggou area (Danshuigou monzogranite and Shenshuitan syenogranite) were analyzed at the State Key

Laboratory for Mineral Deposits Research, Nanjing University, and those of samples from the Gouli area (Niantang syenogranite) were analyzed at the State Key Laboratory of Geological Processes and Mineral Resources, China University of Geosciences, Wuhan. Detailed analytical procedures and methods are presented in Appendix A.

5. Results

5.1. Zircon U–Pb ages

Zircon LA-ICP-MS U–Pb ages from the Danshuigou monzogranite (WDG-1; N36°13'08", E95°55'38"), Shenshuitan syenogranite (WSAG-6; N36°13'04", E95°54'32") and Niantang syenogranite (B1031-1; N35°40'51", E98°22'18") are summarized in Table S1, Appendix B and are illustrated together with representative cathodoluminescence (CL) images of zircons in Figure 3. Zircon grains extracted from the above three samples are all transparent and colorless. The lengths of the zircons from the three intrusions are about 100–300, 80–250, 80–250 μm, with aspect ratios of 4:1 to 1.5:1, 4:1 to 1.5:1, and 5:1 to 1:1, respectively. Oscillatory zonings of most zircons are notable with some zircons show dark and unobvious zonings. In addition, all the zircons show high Th/U ratios (0.42–0.67, 0.52–0.80 and 0.44–0.70, respectively; Table S1, Appendix B), suggesting they are magmatically derived (Wu and Zheng, 2004).

Seventeen analyses of zircons were conducted for the Danshuigou monzogranite and reveal $^{206}Pb/^{238}U$ ages range of ca. 412–425 Ma. These data are plotted in a group on the concordia curve and yield a weighted mean $^{206}Pb/^{238}U$ date of ca. 418 ± 3 Ma (MSWD = 0.62; n = 17; Fig. 3A), which is consistent with previous work (418–420 Ma; Lu et al.,

2013). We thus suggest that the Danshuigou monzogranite formed at ca. 418 Ma. Seventeen spots of zircons were analyzed for the Shenshuitan syenogranite, and yield a $^{206}Pb/^{238}U$ age population of ca. 412–426 Ma, with a weighted mean $^{206}Pb/^{238}U$ age of ca. 418 ± 3 Ma (MSWD = 0.48; n = 17; Fig. 2B), identical with that of the Danshuigou monzogranite. Eighteen analyses of zircons from the Niantang syenogranite yield $^{206}Pb/^{238}U$ ages of 399 to 407 Ma and give a weighted mean $^{206}Pb/^{238}U$ age of ca. 403 ± 2 Ma (MSWD = 0.27; n = 18; Fig. 3C), representing the emplacement age.

5.2. Major and trace element geochemistry

Major and trace element data for all rocks are listed in Table S2, Appendix B and illustrated in Figures 4–6. The Danshuigou monzogranite shows relatively medium SiO_2 (63.5–71.4 wt.%), low CaO (1.66–3.22 wt.%) and MgO (0.70–1.40 wt.%), but high total alkali (K_2O+Na_2O=6.91–8.19 wt.%), $Fe_2O_3^T$ (3.56–6.31 wt.%) and FeO/MgO ratios (4.04–4.58), which are similar to typical A-type granites (Frost, 2001). In the R1-R2 classification diagram, the data mainly fall in the monzogranite field (Fig. 4A; Roche et al., 1980). In the K_2O vs. SiO_2, (Na_2O+K_2O-CaO) vs. SiO_2 and A/NK vs. A/CNK discrimination diagrams (Fig. 4B–D; Maniar and Piccoli, 1989; Frost, 2001), all samples fall in high-K to shoshonitic, alkali-calcic and metaluminous–weakly peraluminous fields. In Harker diagrams, with increasing SiO_2, the CaO, $Fe_2O_3^T$, P_2O_5, Sr, Ba, Zr and Nb contents decrease, with slight increases in FeO_t/MgO (Fig. 5). Rare earth element (REE) patterns of these samples show light rare earth elements (LREEs) enrichment and negative Eu anomalies (Fig. 6A). Trace element spider diagrams display enrichment in Rb, Th, U, La

and Pb and relative depletion in Ba, Nb, Sr, P and Ti (Fig. 6B).

In comparison, the Shenshuitan syenogranite has higher SiO_2 (72.4–78.6 wt.%), K_2O (4.62–5.15 wt.%) and FeO_t/MgO ratios (4.18–5.70), and relatively lower $Fe_2O_3^T$ (0.81–2.28 wt.%), CaO (0.53–1.14 wt.%) and TiO_2 (0.13–0.34 wt.%). In the geochemical classification diagrams, all data fall in the syenogranite field or the boundary between syenogranite and alkali granite, and display high-K, calc-alkalic to alkali-calcic and metaluminous to weakly peraluminous characteristics (Fig. 4). In Harker diagrams, all samples are plotted in a linear trend defined by the Danshuigou monzogranite (Fig. 5); this together with close spatial relationship and identical ages between the two intrusions, suggests they may derive from a similar parental magma via a different degree of crystal fractionation. In chondrite-normalized REE patterns and primitive mantle-normalized trace elements spider diagrams, the Shenshuitan syenogranite shows a similar trend with that of Danshuigou monzogranite, but displays a more notably negative Eu, Ba, Nb, Ta, Sr, P and Ti anomalies, which are similar to the Silurian-Devonian A-type granites from the EKO (Fig. 6C–D).

Samples from the Miantang syenogranite shows high SiO_2 (69.9–74.5 wt.%), K_2O (5.11–6.05 wt.%) and Na_2O (3.23–3.73), medium $Fe_2O_3^T$ (1.90–3.08 wt.%) and CaO (0.82–1.32 wt.%), but much higher FeO_t/MgO ratios (6.68–10.85). In the geochemical classification diagrams, most samples are plotted in the syenogranite area and display shoshonitic, alkali-calcic to alkalic, and metaluminous to weakly peraluminous characteristics (Fig. 4). In Harker diagrams, the CaO, $Fe_2O_3^T$, P_2O_5, Sr, Ba, Zr show weakly negative relationship with SiO_2 (Fig. 5) although the data concentrate in a narrow area,

Journal Pre-proof

which may be due to limited crystal fractionation. The LREEs and LILEs are enriched, and the high field strength elements (HFSEs, e.g., Nb, Ta, Zr, Hf, HREEs) are more enriched than typical Silurian I-type granites (Santougou) from the EKO, although some of the elements display negative anomalies (e.g., Nb, Ta) in trace element spider diagram (Fig. 6E–F).

5.3. Whole rock Sr-Nd isotopes and zircon Lu–Hf isotopes

The Sr–Nd isotope compositions are presented in Table S3, Appendix B and the Nd isotope compositions are further illustrated in Figure 7A. The Danshuigou monzogranite displays $^{87}Rb/^{86}Sr$ ratios of 2.04–6.48 with high initial $^{87}Sr/^{86}Sr$ (0.713519–0.726415; t=418 Ma) and negative $\varepsilon Nd(t)$ (-2.6 – -3.5; t=418 Ma). The Nd two-stage model ages (T_{2DM}^{Nd}) vary from 1369 to 1444 Ma. The Shenshuitan syenogranite shows higher $^{87}Rb/^{86}Sr$ ratios (up to 15.11) and a wide range of initial $^{87}Sr/^{86}Sr$ of 0.705437–0.772205 (t=418 Ma), which are features of many A-type granites (e.g., Wu et al., 2002). It also displays scattered T_{2DM}^{Nd} (1209–1478 Ma) and similar $\varepsilon Nd(t)$ (-3.9 – -0.6) compared with those of Danshuigou monzogranite. The Niankang syenogranite has initial $^{87}Sr/^{86}Sr$ of 0.704960–0.714585 (for comparison with granites from the Wulonggou area we calculated the ratios back to 418 Ma), negative $\varepsilon Nd(t)$ (-5.3 – -4.7) and consistent T_{2DM}^{Nd} (1536–1584 Ma).

The Hf isotopic data of zircons are summarized in Table S4, Appendix B and illustrated in Fig. 7B. $^{176}Hf/^{177}Hf$ of the Danshuigou monzogranite and Shenshuitan syenogranite are of 0.282351–0.282501 and 0.282379–0.282505, respectively. The two intrusions have indistinguishable $\varepsilon Hf(t)$ (-6.3– -1.1 and -5.5 – -1.1, respectively) and Hf

two-stage model ages (T_{2DM}^{Hf}) (1059–1268 Ma and 1064–1252 Ma, respectively), suggesting they were derived from the same source. In contrast, the Niantang syenogranite has higher $^{176}Hf/^{177}Hf$ (0.282527–0.282718) and $\varepsilon Hf(t)$ (-0.1– 6.4), and younger T_{2DM}^{Hf} (973–1272Ma).

6. Discussion

6.1. A Late Silurian–Millde Devonian A-type granite belt

A large amount of I-type granites and minor S- and A-type granites have been revealed in the EKO (Zhang et al., 2005; Mo et al., 2007). The absence of aluminous-rich minerals, such as muscovite and cordierite, in the Danshuigou monzogranite, Shenshuitan and Niantang syenogranites can distinguish these rocks from typical S-type granites. The relatively low Al_2O_3 (Table S2, Appendix B) and negative relationship between P_2O_5 and SiO_2 of the three intrusions (Fig. 5d) also exclude the possibility of an S-type affinity, which commonly shows an opposite trend (Chappell and White, 1992). To distinguish A-type and I-type granites, an integrated discussion of major and trace elements, and a comprehensive comparison between A-type granites and contemporaneous typical I-type granites from the same area are required, especially for units that are highly differentiated (Whalen et al., 1987; King et al., 1997).

In general, A-type granites have higher Na_2O+K_2O, FeOt/MgO, Ga/Al, HFSEs (e.g., Zr and Nb) and lower CaO and Sr than typical I-type granites (e.g., King et al., 1997). All samples from the three intrusions (Danshuigou, Shenshuitan and Niantang) display high total alkali (6.91–9.78 wt.%), high FeOt/MgO (4.04–10.85) and 10,000×Ga/Al (2.51–3.08)

ratios, but low CaO (0.53–3.22 wt.%) contents, which are distinct from the contemporaneous Santougou I-type granite from the EKO (Fig. 1B; Fig. 5A and C), but are consistent with chemical characters of typical A-type granites (Loiselle and Wones, 1979; Whalen et al., 1987; Creaser et al., 1991). In addition, the high Fe* (FeOt/(MgO+FeOt; 0.80–0.92; Table S2) of these samples are chemically similar to ferroan granitoids (Frost, 2001), indicative of an A-type affinity. As to trace elements, the relatively low-silica Danshuigou monzogranite and high-silica Niantang syenogranite show much lower plagioclase-compatible elements, such as Ba and Sr, compared to the Santougou I-type granite (Fig. 5E-F), while the HFSEs (e.g., Zr and Nb) are much higher than typical I-type granites (Fig. 5G-H), assuring their A-type affinity. The relatively high-silica Shenshuitan syenogranite also shows much lower Ba and Sr (Fig. 5E-F), but the HFSEs (e.g., Zr and Nb) are relatively lower (Fig. 5G-H) which obscure the A-type affinity of this syenogranite. However, given that the Shenshuitan syenogranite shares consistent Nd-Hf isotopes with the Danshuigou monzogranite (Fig. 7) and the close spatial relationship between the two intrusions, we suggest that they were from the same or extremely similar magma source. In this context, the A-type affinity (such as high HFSEs) of the Shenshuitan syenogranite was probably erased to some extent by fractional crystallization (King et al., 1997). Samples from the three intrusions show identical REE and trace element patterns with the contemporaneous A-type granites from the EKO, distinguishing themselves from other granite types from this orogen (Fig. 6). The fact that all samples are plotted in the within-plate field in the Rb vs. Yb+Nd space (Pearce et al., 1984) and in the A-type granite

area in the discrimination diagrams (Whalen et al., 1987) also support the above conclusion (Fig. 8).

On the other hand, A-type granites are characterized by anhydrous, high-T and low-P properties (e.g., Loiselle and Wones, 1979), which can also be used to separate themselves from other types of granites. Zircon saturation thermometer (T_{Zr}) based on bulk-rock composition can offer a minimum estimate of magma temperature if the magma is undersaturated in Zr (Watson et al., 2006). The absence of inherited zircons in the three intrusions indicates that the primary magmas were undersaturated in Zr (Fig. 3; Miller et al., 2003). In this case, the high T_{Zr} of the Danshuigou monzogranite (841–884 °C; Table S2, Appendix 2; Fig. 9A) and Niantang syenogranite (811–857 °C; Table S2, Appendix 2; Fig. 9A) imply a high-temperature origin. The relatively lower T_{Zr} of the Shenshuitan syenogranite (775–797 °C; Table S2, Appendix 2; Fig. 9A) could be due to some extent crystal fractionation given the higher silica content compared to that of the Danshuigou monzogranite, and thus we also contend to its high-temperature origin. As for the pressure of magma, experimental studies indicate that ratios of some major elements (i.e., $Al_2O_3/(FeOt+MgO+TiO_2)$) can provide an estimate of the pressure of magma (Patino Douce, 1999). The low $CaO/(FeOt+MgO+TiO_2)$ and $Al_2O_3/(FeOt+MgO+TiO_2)$, and high $(K_2O+NaO_2)/(FeOt+MgO+TiO_2)$ ratios of the three intrusions indicate that the magmas formed in a low-pressure condition (Patino Douce, 1999), which is consistent with that all samples are plotted along low-pressure curves in the $CaO/(FeOt+MgO+TiO_2)$ vs. $CaO+FeOt+MgO+TiO_2$ diagram (Fig. 9B). In addition, the pronounced negative Ba, Sr and

Journal Pre-proof

Eu anomalies and flat HREE patterns which indicate the preference of plagioclase and absence of residual garnet, favor a low-pressure condition (Fig. 6). Moreover, the pervasive perthites in all rocks also agree well with the high-temperature and low-pressure conditions. With regard to the water contents of the magmas, a special mineral crystallization sequence of the studied granites should offer some preliminary information. Biotite from the Danshuigou monzogranite, Shenshuitan and Niantang syenogranites are interstitial with the feldspar and quartz (Fig. 2). This phenomenon denotes that the biotite stabilized late in the crystallization sequence as the water was gradually enriched and thus indicate that the primary magmas are likely to be anhydrous (King et al., 1997). In summary, anhydrous, high-temperature and low-pressure characteristics of these magmas further solidify their A-type affinity.

From a regional perspective, numerous Silurian-Devonian granites have been reported in the EKO (Appendix C). These granites share similar elemental and isotopic signatures (Figs 4–7), as well as high-temperature and low-pressure nature (Fig. 9), with the studied A-type granites, assuring their A-type granite attribute (Fig. 8). Although these A-type granites are spatially sparse, they spread in the entire EKO, from the very western Baiganhu, through the central Binggou, to the eastern Gouli (Niantang), forming an A-type granite belt (Fig.1b), which should imply extensive A-type magmatism during this period in the EKO.

6.2. Petrogenesis

A-type granites with complex compositional variations could be derived from different sources via various processes. Four plausible models have been proposed for the formation

of A-type granites: (1) fractional crystallization of mantle-derived magma (e.g., Turner et al., 1992), (2) mixing between crust and mantle-derived magmas (Yang et al., 2006), (3) partial melting of continental granulitic metasedimentary rocks (Huang et al., 2011) or igneous rocks (e.g., Whalen et al., 1987), and (4) partial melting of underplated mafic (basaltic) rocks (Wu et al., 2002) or calc-alkaline granitoids in the crust (e.g., Creaser et al., 1991).

Compared with the depleted mantle-derived MORB in the EKO, the notably lower εNd(t) and εHf(t) of the studied A-type granites preclude depleted mantle as the source region of these A-type granites (Fig. 7). Although enriched mantle defined by contemporaneous mafic rocks from the Huxiaoqin and Yuejinshan in the EKO (Fig. 1B) show similar isotopic characteristics with the studied A-type granites (Fig. 7; Liu et al., 2012; Liu et al., 2013), the anhydrous attribute of the studied rocks suggest that the water-rich enriched mantle is unlikely to be the source. Several lines of additional evidence below further support the above conclusion: (1) A-type granites from the western Wulonggou and eastern Gouli areas display high SiO_2 (63.5–78.6 wt. %) and extremely low MgO (0.13–1.4 wt. %), which are unlikely to be directly generated by fractional crystallization of mantle-derived magma, since rocks derived directly from mantle tend to be mafic to high-Mg andesitic (Baker et al., 1995; Ding et al., 2014); (2) extensive crystallization of mantle-derived magma would produce a large amount of coeval mafic and/or intermediate igneous rocks (Turner et al., 1992), which is not the case in the Wulonggou and Gouli areas; (3) mantle-derived A-type granites normally show peralkaline signature that is inconsistent with the metaluminous – weakly peraluminous characteristic

of the studied rocks (Fig. 4D; King et al., 1997). Additionally, based on the lack of evidence of mixing, such as magmatic enclaves or bimodal distribution of εNd(t) and εHf(t) of the three intrusions, we also do not favor this genetic model for our studied rocks (Yang et al., 2006). In fact, the high Y/Nb ratios (>2) and A_2-type nature of these rocks as shown in Figure 10 imply that the sources of these aluminous A-type granites are most likely continental crust (Eby, 1990; 1992). Thus, we suggest that the A-type granites from the Wulonggou and Gouli areas may be generated by the partial melting of continental crustal rocks such as granulitic residue, underplated mafic rocks or granitoids (Whalen et al., 1987; Creaser et al., 1991; Wu et al., 2002; Huang et al., 2017).

Magmas derived from granulitic metasedimentary rocks usually show high Al_2O_3 and low Na_2O+K_2O, thus exhibiting peraluminous signature (Chappell and White, 1992), which is inconsistent with the metaluminous-slightly peraluminous signature of the A-type granites from the Wulonggou and Gouli areas (Fig. 4C–D). In addition, the HFSEs and HREEs of the studied A-type granites are much higher than contemporaneous sediment-derived S-type granites in the EKO, suggesting different sources of these A-type granites (Fig. 6; Shi et al., 2016). More importantly, the εNd(t) and εHf(t) values of the studied A-type granites are much higher than coeval S-type granites from the Jinshuikou and metasedimentary rocks from the basement of the EKO, arguing against that the studied A-type granites are derived from granulitic metasedimentary rocks (Fig. 7). Partial melting of granulitic igneous residue should generate magmas depleted in alkalis that had escaped from the source region in previous melt extraction events (Creaser et al., 1991), which

contradicts the high Na_2O+K_2O of the studied A-type granites. In addition, earlier melt-extraction of an igneous source is likely to yield residues enriched in Ca and Al and depleted in K and Si and melt from this residual source will inherit these signatures, which are inconsistent with the relative low Ca and Al and high K and Si of the studied A-type granites (Table S2, Appendix B; Creaser et al., 1991). Moreover, a residual source which usually contains pyroxene (amphibole) should have low Fe/Mg ratio and is unlikely to generate the high Fe/Mg A-type granites in our study (Fig. 5C; Creaser et al., 1991).

Consequently, partial melting of underplating basaltic rocks or calc-alkaline granitoids (or extrusive counterparts) from the continental crust would be plausible to produce the A-type granites in our study. The protoliths of underplating basaltic sources could be derived from a depleted mantle or enriched mantle. Depleted mantle-derived basalts (tholeiites) should hold extremely depleted isotopic signatures as indicated by the basalts from the Buqingshan (Fig. 7) and thus would result in the magmas from them have similar depleted characteristics, which are inconsistent with the relatively enriched isotopic signatures of the studied A-type granites (Fig. 7). Enriched mantle-derived basalts are also unlikely to be the sources, since these basalts contain a significant volume of amphiboles as evidenced by the coeval intrusive counterparts in the Yuejinshan and Huxiaoqin areas (Liu et al., 2012; Liu et al., 2013) and should be less probable to produce the studied anhydrous A-type granites. In addition, experimental studies have revealed that granitic melts from the dehydration partial melting of mafic rocks should be compositionally similar to calc-alkaline I-type granites with high Al_2O_3, CaO and Na_2O/K_2O and low

$(K_2O+Na_2O)/Al_2O_3$ (Rapp and Watson, 1995), which is inconsistent with the compositions of the studied A-type granites. More importantly, coeval typical I-type granites which were derived from mafic rocks in the EKO show much lower HREE and HFSE than the studied A-type granites, suggesting different sources for the A-type granites (Fig. 6; Zhang et al., 2014).

It is suggested that the geochemical composition and water contents of A-type granites could be produced by partial melting of calc-alkaline granitoids (Creaser et al., 1991). Experimental studies have also evidenced that 15–40 % partial melting of calc-alkaline granitoids under a high-temperature and low-pressure condition should generate metaluminous–slightly peraluminous A-type melt (Douce and Alberto, 1997), which coincide with the high-temperature and low-pressure nature and metaluminous–slightly peraluminous signature of the studied A-type granites. More importantly, earlier granitoid rocks in the EKO have wide ranges of εNd(t) and εHf(t) that bracket those values of the studied A-type granites, further supporting the above conclusion (Fig. 7). The reported granitoid rocks in the EKO that intruded before the Late Silurian are dominated by the Proterozoic granitic gneisses (Chen et al., 2015; He et al., 2016) and Ordovician-Silurian granitoids (e.g., Li et al., 2015; Zhou et al., 2016; Chen et al., 2016). The Proterozoic granitic gneisses typically exhibit a peraluminous signature (e.g., He et al., 2016) and thus are unlikely the main sources of the low-Al_2O_3 A-type granites. Moreover, these granitic gneisses (such as the Bokalike gneiss) display diagnostically low εHf (t) and thus, are impossible to be the main sources of the studied A-type granites with relatively higher εHf

(t) (Fig. 7 B). On the other hand, Ordovician-Silurian granitoids prevail in the EKO, such as those in the Santougou (Zhang et al., 2014), Yikehalaer (Li et al., 2015), Aowade (Chen et al., 2016) and Zhiyu (Zhou et al., 2016) (Fig. 1B). These rocks are calc-alkaline and metaluminous to slightly peraluminous (e.g., Li et al., 2015), and thus could be ideal sources for the studied A-type granites (Douce and Alberto, 1997). In particular, these Ordovician-Silurian granitoids, which are recommended to be mainly derived from enriched mantle or oceanic crust (e.g., Zhang et al., 2014; Li et al., 2015; Chen et al., 2016; Zhou et al., 2016), display similar εNd(t) and εHf(t) with the A-type granites from the Wulonggou and Gouli areas (Fig. 7), which solidify the above conclusion. Besides, it should be noticed that the A-type granites from the Wulonggou have lower εHf(t) than that of A-type granites from the Gouli (Fig. 7B) and the latter of which show notable decoupling between εNd(t) and εHf(t). The lower εHf(t) of the A-type granites from the Wulonggou could be caused by minor involvement of Proterozoic crustal materials in the sources. The distinct ages (418 vs.403 Ma) between the A-type granites from the two regions may also lead to their differences in Hf isotopes, since as delamination ongoing (discussed in section 6.3), more depleted materials (Asthenosphere mantle) may be added to the crust and may be included in the formation of the young A-type granites. However, considering the errors of the data, the <epsilon>Nd(t) values of the young or old A-type granites are identical (Fig. 7A and Table S3, Appendix B), implying that distinct ages are unlikely the main reason leading to the different Hf isotopes between the plutons from the Wulonggou and Gouli. As shown in Fig. 1 and Fig. 7B, the Santougou granitoids (no Hf isotopic data reported) and the

Yuejinshan mafic rocks (Hf isotopic data reported), both of which are from an neighboring area of the Wulonggou, are likely to have similar <epsilon>Hf(t) values in view of their similar source (enriched mantle; Liu et al., 2012; Zhang et al., 2014). The <epsilon>Hf(t) values of the Yuejinshan mafic rocks (as well as that speculated for the Santougou granitoids) are notably lower than that of granitoids from the Gouli area (Aowade; Chen et al., 2016), which suggest inhomogeneity of the source region of the studied A-type granites may lead to the distinct Hf isotopes between the Wulonggou and Gouli pluton. The decoupling of the εNd(t) and εHf(t) of the Niantang A-type granite may also inherit from their source, considering that Ordovician-Silurian granitoids from the Gouli area show the same feature (Fig. 7; Chen et al., 2016). Consequently, we contend that the studied A-type granites should be formed via the partial melting of Ordovician-Silurian granitoids with/without the involvement of Proterozoic crustal materials. Considering all Late Silurian - Middle Devonian A-type granites from the EKO share similar chemical signatures with the studied A-type granites (Figs. 4-7), we favor similar sources for these rocks.

6.3. Tectonic implications for the Proto-Tethys evolution

The ophiolites that occur in the Qingshuiquan (Fig. 1B; 518–481 Ma; Yang et al., 1996; Wei, 2015) and Changshishan (537 Ma; Qi et al., 2016) from the Central East Kunlun Suture zone, and Heishan (486 Ma; Meng et al., 2015) and Bashikangkuo (501 Ma; Zheng et al., 2016) from the Northern East Kunlun Suture zone indicate that the Proto-Tethyan Ocean (herein referred to as the Central Kunlun Ocean) and accompanied Qimantag back-arc basin opened no later than the Cambrian. The arc-related rocks, such as the

hornblende diorite from the Xiadawu (447–451 Ma; Xiong et al., 2015), granodiorite from the Aowade (Fig. 1B; 454 Ma; Chen et al., 2016), quartz diorite from the Kekesha (515 Ma; Zhang et al., 2010) and Granodiorite from the Yikehalaer (436 Ma; Li et al., 2015) imply that the oceanic subduction should have initiated during Cambrian and continued to the Early Silurian. In contrast, conflicting views are proposed for the late-stage evolution of the Proto-Tethyan Ocean. The main difference lies in whether the Proto-Tethyan Ocean closed during the Silurian-Devonian (Zhang et al., 2014; Song et al., 2018) or continued to Carboniferous (inherited by the Paleo-Tethys Ocean) (Zhou et al., 2016; Dong et al., 2018). To clarify the above debate, the Silurian-Devonian rocks could offer some information.

The Early Devonian A-type granites from the western Wulonggou and Eastern Gouli areas, together with the coeval A-type granites in the EKO, compose an Late Silurian–Middle Devonian A-type granite belt (Fig. 1C; ~425–385 Ma; Appendix C), which indicates large-scale magmatic activity during this period. This expansive A-type magmatism (~425–385 Ma; Fig. 1C) indicates regional extension that could be post-collisional or anorogenic (e.g., rift) (e.g., Whalen et al., 1987; Eby, 1992; Wu et al., 2002). Granites of A-type affinity can be subdivided into two chemical groups, i.e. A1- and A2-type (Eby, 1992). The A1-type granites represent magmas from oceanic-island basalts and emplacement in anorogenic setting (e.g., rift), with the A2-type granites being considered to be derived from the crust that has been gone through a cycle of subduction and continent-continent collision; that is to say, A2-type granites are formed during post-collisional orogenesis (Eby, 1992). All data from the Late Silurian–Middle Devonian

A-type granites fall in the A_2-type granite field in the Rb/Nb –Y/Nb and Nb-Y-3Ga diagrams (Fig. 10), suggesting a post-collisional setting for the Late Silurian–Middle Devonian A-type granites in the EKO. In the Rb vs. Y+Nb tectonic discrimination diagram (Fig. 8A), all these A-type granites are plotted in the area defined by post-collisional granites (Whalen et al., 1987), further supporting the above speculation. Further, the aluminous and high-K calc-alkaline signatures of these A-type granites are consistent with those of granites occurring in orogenic belts and should be related to the end of collision (e.g., Bonin, 2004). Apart from the evidence above, the Late Silurian–Middle Devonian molasses formation (423–400 Ma; Lu et al., 2010) and the contemporaneous mafic-ultramafic rocks in the EKO also indicate a post-collision extensional event that is likely caused by delamination and related asthenosphere upwelling (e.g., Li et al., 2015; Li et al., 2018). Taken together, the evidence noted above indicates a post-collisional extensional setting in the EKO during the Late Silurian and Middle Devonian.

Researchers who hold the opinion that the Proto-Tethyan Ocean continued to the Carboniferous consider the South East Kunlun Terrain is composed of a Cambrian – Early Paleozoic accretionary complex and the Silurian – Devonian extension was caused by closure of the Qimantag back-arc basin and subsequent delamination along the Northern East Kunlun Suture Zone (Zhou et al., 2016; Dong et al., 2018). However, as shown in Fig. 1, Silurian – Devonian A-type granites are distributed both along the Central and the Northern East Kunlun Suture zones (Fig. 1B), so does the contemporaneous molasses formation (e.g., Lu et al., 2010) and mafic-ultramafic rocks (e.g., Li et al., 2015; Li et al.,

2018). These together indicate extension and delamination along the two suture zones (Fig. 11). In other words, the Proto-Tethyan Oceanic closure and subsequent continental collision should have terminated prior to the Late-Silurian. Several pieces of other evidence also suggest the protracted subduction model (Proto-Tethyan Ocean continued to Carboniferous) should be unlikely true: (1) eclogites occurring along the two sutures indicating close of the Proto-Tethyan Ocean and its back-arc basin before Devonian (Fig. 1; Appendix C); (2) widespread Proterozoic metamorphic rocks (Wang et al., 2007; He et al., 2016) and Proterozoic T_{2DM}^{Nd} and T_{2DM}^{Hf} of many granitoids in the Southern East Kunlun Terrain (Zhou et al., 2016; Chen et al., 2016) are inconsistent with a Cambrian – Early Paleozoic accretionary complex for this terrain; (3) ophiolites along the Central East Kunlun Suture zone (SSZ-type; 555 – 456 Ma) (Yang et al., 1996; Li, 2008; Wei, 2015) and Southern East Kunlun Suture zone (MOR-type; 535 – 308 Ma) (Chen et al., 2001; Yang et al., 2004; Li, 2008; Liu et al., 2011) show distinct types, which are unlikely formed by a continued subduction. Taken together, we suggest that the closure of the Proto-Tethyan Ocean and accompanying Qimantag back-arc basin should be earlier than the Late Silurian, and the post-collisional extension and delamination should occur during the Late Silurian – Middle Devonian (~425-385 Ma; Fig. 11). As to the collision and the possible slab break-off (Fig. 11), we propose that these events occurred during Late Silurian-425 Ma, considering: (1) there is a transition from arc-magmatic rocks to A-type granites during this period (e.g., Zhang et al., 2014; Li et al., 2015); (2) many eclogites with age between 440-425 Ma occurred in the EKO (Appendix C).

Journal Pre-proof

6.4. Implications for the evolution of northern Gondwana

From a regional perspective, a recent study has revealed that the EKO was a part of a unified terrane that also consisted of the West Kunlun Block, Central Altyn Block, Central Qilian Block and North Qinling Block during the Late Proterozoic–Ordovician (Fig. 12; Li et al., 2018 and references therein). Detrital zircon age spectra of Proterozoic–Early Paleozoic strata from these blocks/terranes suggest that all of them had a close affinity with the Arabia Block, the India Block or the Australia block of northern Gondwana (Li et al., 2018 and references therein). An extensive ocean (Proto-Tethyan Ocean or a branch of this Ocean), which has been evidenced by the occurrences of contemporaneous ophiolites from the Qinling (534–457 Ma; Dong et al., 2011 and references therein), Qilian (550–496 Ma; Song et al., 2014 and references therein), EKO (518–481 Ma; Yang et al., 1996; Liu et al., 2011b; Wei, 2015) and West Kunlun Orogen (525–489 Ma; e.g., Zhang et al., 2004; Huang et al., 2014), developed along northern Gondwana during the Late Proterozoic–Ordovician and separated these blocks/terranes from Gondwana. In this context, the Late Silurian–Middle Devonian A-type granite belt in the EKO which indicates the closure of the Proto-Tethyan Ocean should imply that the EKO, as well as the unified terrane, has amalgamated into northern Gondwana or other microcontinents splitting from northern Gondwana (development of Paleo-Tethys Ocean) no later than Late Silurian (Fig. 12). This speculation should be true when taking into account the contemporaneous magmatic pattern of those blocks/terranes that were included in the united terrane. Apart from the recognition of the Late Silurian–Middle Devonian (425–385 Ma) A-type granite belt from the EKO,

contemporaneous post-collisional magmatic rocks have been identified in adjacent terranes, such as the ~405 Ma A-type granites and lamprophyre dikes from the West Kunlun Orogen (Yuan et al., 2002), the 424–385 Ma A-type granites from the Altyn Block (Wang et al., 2014; Kang et al., 2015 and references therein), the 400–390 Ma S-type granites from the Qilian (Song et al., 2014 and references therein) and the 441–409 Ma I-S-type monzogranites or syenogranites from the Qinling (Wang et al., 2013 and references therein). Although the chemical signatures of these rocks vary, they reflect a common tectonic regime (post-collisional environment) during the Silurian–Devonian. As such, the Proto-Tethyan Ocean between the unified terranes and northern Gondwana (or microcontinents from it as the Paleo-Tethys Ocean developed) had closed, which resulted in this united terrane amalgamated with northern Gondwana or Gondwana-derived microcontinents during the Silurian–Devonian (Fig. 12).

7. Conclusions

(1) The Early Devonian A-type granites from the western Wulonggou and the Eastern Gouli areas in the EKO were formed by partial melting of the Ordovician-Silurian granitoids.

(2) The closure of the Proto-Tethyan Ocean and the subsequent collision and possible slab break-off should be earlier than ~425 Ma, after which a post-collisional extensional event and delamination initiated and continued to ca. 385 Ma.

(3) The EKO and the adjacent terranes should be amalgamated into northern

Gondwana or Gondwana-derived microcontinents as a result of the closure of the Proto-Tethyan Ocean during the Silurian–Devonian.

Acknowledgments

This research was jointly supported by the Fundamental Research Funds for the Central Universities, China University of Geosciences (Wuhan) (CGL17043), the Funds from the East China University of Technology (DHBK2018009 and GJJ180387), and the China Geological Survey (12120114081401, 1212011400701). Lebing Fu acknowledges the China Scholarship Council. We appreciate the valuable help of Jun Tan, Shaoqing Zhao, Zhen Wang, Xiaolong Wang and Yilong Wang from the CUG during the fieldwork.

Journal Pre-proof

Figure captions

Fig. 1 (A) Sketch map of the Qinghai-Tibetan plateau showing dominated blocks/terranes in the west of China (after Chen et al., 2017); (B) Simplified geological map of the EKO, showing the localities of the study areas (after Chen et al., 2017); (C) Geological map of the Wulonggou area (after unpublished geological report); (D) Geological map of the Gouli area (after unpublished geological report). TRMB-Tarim block; ALSB-Alashan block; INDB-Indian block; YZB-Yangtze block; NEKT-Northern East Kunlun Terrane; SEKT-Southern East Kunlun Terrane. Locations and ages of the Silurian–Devonian A-type granites from the Baiganhu, Huanglongou, Houshugou, Binggou, Helegangnaren, Lalingzaohuo, Xiarihamu, Wulonggou and Niantang are also shown in Fig. 1B, so as to eclogites from the Wenquan, Garidang, Kuhete, Zongjia, Dagele, Sutuhai and Xiarihamu (Appendix C). The zircon U-Pb ages for the Qingshuiquan and Tatuo ophiolites in the Gouli area are from Wei(2015) and that of Devonian gabbro in the Wulongou area is from our unpublished data.

Fig. 2. Photographs of the Danshuigou monzogranite (A, B, C), the Shenshuitan syenogranite (D, E, F) and the Niantang syenogranite (G, H, I). Bi–biotite; Pl–plagioclase; Kf–Alkali-feldspar; Qz–quartz; Hb-hornblende.

Fig. 3. Representative CL images and U–Pb concordia plots of Danshuigou monzogranite

(A), Shenshuitan syenogranite (B) and Niantang syenogranite (C). The locations of U-Pb ages (red solid circles) and Lu-Hf isotope (yellow dashed circles) analyses are also shown on the corresponding CL images. MSWD: mean square of weighted deviation.

Fig. 4. Plots of (A) R1 versus. R2 (after Roche et al., 1980); (B) K_2O versus SiO_2 (after Middlemost, 1985), (C) Na_2O+K_2O-CaO versus SiO_2 (after Frost, 2001) and (D) A/NK [molar ratio $Al_2O_3/(Na_2O+K_2O)$] versus A/CNK [molar ratio $Al_2O_3/(CaO+ Na_2O+K_2O)$] (after Maniar and Piccoli, 1989) for the Danshuigou monzogranite, Shenshuitan syenogranite and Niantang syenogranite. The data sources of the Silurian–Devonian A-type granites are listed in Appendix C. R1=4Si-11(Na+K)-2(Fe+Ti); R2=6Ca+2Mg+Al.

Fig. 5. Harker diagrams of selected major and trace elements for Danshuigou monzogranite, Shenshuitan syenogranite and Niantang syenogranite. The data from the Silurian Santougou I-type granites (Zhang et al. 2014) in the EKO are also shown for comparison. The data sources of the Silurian–Devonian A-type granites are listed in Appendix C.

Fig. 6. Primitive mantle-normalized trace element spiderdiagrams and chondrite-normalized rare earth element patterns for the Danshuigou monzogranite (A–B), Shenshuitan syenogranite (C–D) and Niantang syenogranite (E–F). Primitive mantle and chondrite normalizing values are from Sun and McDonough(1989). The data for I-type granitoids are

from Santougou (Zhang et al., 2014) and those of S-type granites are from Heishan (Shi et al., 2016) as shown in Fig. 1B. The data sources of the Silurian–Devonian A-type granites are listed in Appendix C.

Fig. 7. Plots of (A) εNd(t) versus T(Ma) and (B) εHf(t) versus T(Ma). Data of Buqingshan ophiolite (Bian et al., 2004), Jinshuikou granulite xenoliths (Long, 2004), Jinshuikou crust-derived S-type granite (Yu et al., 2005), Dulan oceanic eclogite (Zhang et al., 2016), Bokalike genesis (He et al., 2016), Yuejinshan (Liu et al., 2012) and Huxiaoqin (Liu et al., 2013) enriched-mantle derived gabbro, Santougou (Zhang et al., 2014), Aowade (Chen et al., 2016), Yikehalaer (Li et al., 2015) and Zhiyu (Zhou et al., 2016) Ordovician-Silurian granitoids and Silurian – Devonian A-type granites (Yugouzi, Binggou and Houtougou; the data sources of these A-type granites are listed in Appendix C) from the EKO are also shown for comparison.

Fig. 8. Plots of: (A) Y+Nb versus Rb; (B) 1000Ga/Al versus Zr; (C) 1000Ga/Al versus FeOt/MgO and (D) Zr+Nd+Ce+Y versus FeO_t/MgO for the Danshuigou monzogranite, Shenshuitan syenogranite and Niantang syenogranite to distinguish them from I-, S-, M-type granites (after Whalen et al., 1987). syn-COLG and post-COLG: syn- and post-collisional granites. WPG: within-plate granites. VAG: volcanic arc granites. ORG: ocean-ridge granites. I, S, M and A represent I-, S-, M- and A-type granites respectively. FC

denotes fractionated granites. OGT represents unfractionated I-, S-, M-granites. The data sources of the Silurian–Devonian A-type granites are listed in Appendix C. The data of highly-fractionated I-type granites are from Zhang et al., (2013).

Fig. 9. SiO_2 versus T_{zr} (°C) (A) and $CaO+FeO_t+MgO+TiO_2$ versus $CaO/(FeO_t+MgO+TiO_2)$ (B) diagrams for the Danshuigou monzogranite, Shenshuitan syenogranite and Niantang syenogranite (after Patino Douce, 1999; Watson et al., 2006). The boundary between hot granites and cold granites in Fig. 9A is after Miller et al. (2003). MAGS: metaluminous 'A-type' granites; CAGS: calc-alkaline granites; FBRs: rhyolites associated with flood basalts. The solid lines labeled with LP and HP are reaction curves as expected for melt compositions that would be produced by hybridization of high-Al olivine tholeiite with metagreywacke at low pressure (LP, ≤5 kbar) and high pressure (HP, 12 to 15 kbar) respectively (Patino Douce, 1999). The dash-dot lines are reaction curves for low-pressure hybridization of calc-alkaline granites with high-Al olivine tholeiite (Patino Douce, 1999). The Silurian I-type granites from the Santougou are also shown for composition. The data sources of the Silurian–Devonian A-type granites are listed in Appendix C.

Fig. 10. Rb/Nb-Y/Nb (A) and Nb-Y-3Ga (B) diagrams for the Danshuigou monzogranite, Shenshuitan syenogranite and Niantang syenogranite (after Eby, 1992). A1 and A2 represent two subgroups of A-type granite defined by Eby(1992). The data sources of the Silurian–Devonian A-type granites are listed in Appendix C.

Fig. 11. Schematic cartoon showing Silurian – Devonian tectonic evolution of the East Kunlun orogen. Plutons in red represent medium-felsic intrusion, green mafic dikes, blue A-type granites, and purpose mafic-ultramafic rocks. The purple areas in the CEKS and the NQS represent ophiolites. NQS-North East Kunlun Suture Zone; CEKS-Central East Kunlun Suture Zone; CEKT-Central East Kunlun Terrain; SEKT- Southern East Kunlun Terrain;

Fig. 12. Devonian ocean-continent configuration of northern Gondwana showing the position of the East Kunlun Orogen (after Li et al., 2018). The post-collisional intrusions are also shown and for related references see text. WKL-West Kunlun; EKO-East Kunlun Orogen; QD-Qaidam Block; CAL-Central Altyn Block; CQL-Central Qilian Block; NQL-North Qinling Block; SQT-South Qiangtang Block; NQT- North Qiangtang Block; SI-Sibumasu Block; IC-Indochina Block; SP-Songpan-Ganze Block; LS-Lhasa Block; CA-Cathaysia Block; YZ-Yangtze Block; BJ-Bureya-Jiamusi Block.

Journal Pre-proof

References

Baker, M.B., Hirschmann, M.M., Ghiorso, M.S., Stolper, E.M., 1995. Compositions of near-solidus peridotite melts from experiments and thermodynamic calculations. Nature 375 (6529), 308.

Bian, Q.T., Li, D.H., Pospelov, I., Yin, L.M., Li, H.S., Zhao, D.S., Chang, C.F., Luo, X.Q., Gao, S.L., Astrakhantsev, O., Chamov, N., 2004. Age, geochemistry and tectonic setting of Buqingshan ophiolites, North Qinghai-Tibet Plateau, China. Journal of Asian Earth Sciences 23 (4), 577-596.

Bonin, B., 2004. Do coeval mafic and felsic magmas in post-collisional to within-plate regimes necessarily imply two contrasting, mantle and crustal, sources? A review. Lithos 78 (1), 1-24.

Bonin, B., Azzouni-Sekkal, A., Bussy, F., Ferrag, S., 1998. Alkali-calcic and alkaline post-orogenic (PO) granite magmatism: petrologic constraints and geodynamic settings. Lithos 45 (1), 45-70.

Chappell, B.W., White, A.J.R., 1992. I- and S-type granites in the Lachlan Fold Belt. Earth and Environmental Science Transactions of the Royal Society of Edinburgh 83 (1-2), 1-26.

Chen, J., Wei, J., Fu, L., Li, H., Zhou, H., Zhao, X., Zhan, X., Tan, J., 2017. Multiple sources of the Early Mesozoic Gouli batholith, Eastern Kunlun Orogenic Belt, northern Tibetan Plateau: Linking continental crustal growth with oceanic subduction. Lithos 292-293, 161-178.

Journal Pre-proof

Chen, J.J., Fu, L.B., Wei, J.H., Tian, N., Xiong, L., Zhao, Y.J., Zhang, Y.J., Qi, Y.Q., 2016. Geochemical characteristics of Late Ordovician granodiorite in Gouli area, Eastern Kunlun Orogenic Belt, Qinghai province: Implications on the evolution of Proto-Tethys Ocean. Earth Science 41 (11), 1863-1882 (in Chinese with English abstract).

Chen, Y.X., Pei, X.Z., Li, R.B., Li, Z.C., Pei, L., Liu, C.J., Yang, J., 2014. Geochemical characteristics and tectonic significance of meta-sedimentary rocks from Naij Tal group, eastern section of East Kunlun. Geoscience 28 (03), 489-500 (in Chinese with English abstract).

Chen, Y.X., Pei, X.Z., Li, Z.C., Li, R.B., Liu, C.J., Chen, G.C., Pei, L., Wei, B., 2015. Geochronology, geochemical features and geological significance of the granitic gneiss in Balong area, East Section of East Kunlun. Acta Petrologica Sinica 31 (08), 2230-2244 (in Chinese with English abstract).

Chen, L., Sun, Y., Pei, X.Z., Gao, M., Tao, F., Zhang, Z.Q., Chen, W., 2001. Northernmost Paleo-Tethyan oceanic basin in Tibet: geochronological evidence from 40Ar/39Ar age dating of Dur'ngoi ophiolite. Chinese Science Bulletin 46, 1203-1205.

Creaser, R.A., Price, R.C., Wormald, R.J., 1991. A-type granites revisited: Assessment of a residual-source model. Geology 19, 163-166.

Ding, Q.F., Jiang, S.Y., Sun, F.Y., 2014. Zircon U–Pb geochronology, geochemical and Sr–Nd–Hf isotopic compositions of the Triassic granite and diorite dikes from the Wulonggou mining area in the Eastern Kunlun Orogen, NW China: petrogenesis and tectonic implications. Lithos 205, 266-283.

Journal Pre-proof

Dong, Y., He, D., Sun, S., Liu, X., Zhou, X., Zhang, F., Yang, Z., Cheng, B., Zhao, G., Li, J., 2018. Subduction and accretionary tectonics of the East Kunlun orogen, western segment of the Central China Orogenic System. Earth-Science Reviews 186, 231-261.

Dong, Y., Sun, S., Liu, X., He, D., Zhou, X., Zhang, F., Yang, Z., Zhou, D., 2019. Geochronology and geochemistry of the Yazidaban ophiolitic mélange in Qimantagh: constraints on the Early Paleozoic back-arc basin of the East Kunlun Orogen, northern Tibetan Plateau. Journal of the Geological Society 176 (2), 306-322.

Dong, Y.P., Zhang, G.W., Neubauer, F., Liu, X.M., Genser, J., Hauzenberger, C., 2011. Tectonic evolution of the Qinling orogen, China: Review and synthesis. Journal of Asian Earth Sciences 41 (3), 213-237.

Douce, P., Alberto, E., 1997. Generation of metaluminous A-type granites by low-pressure melting of calc-alkaline granitoids. Geology 25 (8), 743.

Eby, G.N., 1990. The A-type granitoids: A review of their occurrence and chemical characteristics and speculations on their petrogenesis. Lithos 26 (1–2), 115-134.

Eby, G.N., 1992. Chemical subdivision of the A-type granitoids: Petrogenetic and tectonic implications. Geology 20 (7), 641.

Frost, B.R., 2001. A geochemical classification for granitic rocks. Journal of Petrology 42 (11), 2033-2048.

He, D.F., Dong, Y.P., Liu, X.M., Yang, Z., Sun, S.S., Cheng, B., Li, W., 2016. Tectono-thermal events in East Kunlun, Northern Tibetan Plateau: evidence from zircon U–Pb geochronology. Gondwana Research 30, 179-190.

Journal Pre-proof

He, D.F., Dong, Y.P., Zhang, F.F., Yang, Z., Sun, S.S., Cheng, B., Zhou, B., Liu, X.M., 2016. The 1.0 Ga S–type granite in the East Kunlun Orogen, Northern Tibetan Plateau: Implications for the Meso–to Neoproterozoic tectonic evolution. Journal of Asian Earth Sciences 130, 46-59.

Huang, C.Y., Wang, H., Liu, J.P., Hu, J., Mu, S.L., Qiu, Z.W., 2014. Geological, geochemical features and structure significance of Kegang ophiolite, West Kunlun. Geochimica 43 (06), 592-601 (in Chinese with English abstract).

Huang, H.Q., Li, X.H., Li, W.X., Li, Z.X., 2011. Formation of high δ18O fayalite-bearing A-type granite by high-temperature melting of granulitic metasedimentary rocks, southern China. Geology 39 (10), 903-906.

Kang, L., Xiao, P., Gao, X., Xi, R., Yang, Z., 2015. Age, petrogenesis and tectonic implications of Early Devonian bimodal volcanic rocks in the South Altyn, NW China. Journal of Asian Earth Sciences 111, 733-750.

King, P.L., White, A.J.R., Chappell, B.W., Allen, C.M., 1997. Characterization and origin of aluminous A-type granites from the Lachlan Fold Belt, Southeastern Australia. Journal of Petrology 38 (3), 371-391.

Li, C., Zhang, Z., Li, W., Wang, Y., Sun, T., Ripley, E.M., 2015. Geochronology, petrology and Hf–S isotope geochemistry of the newly-discovered Xiarihamu magmatic Ni–Cu sulfide deposit in the Qinghai–Tibet plateau, western China. Lithos 216-217, 224-240.

Li, L., Sun, F., Li, B., Li, S., Chen, G., Wang, W., Yan, J., Zhao, T., Dong, J., Zhang, D., 2018. Geochronology, geochemistry and Sr-Nd-Pb-Hf isotopes of No. I complex from

the Shitoukengde Ni-Cu sulfide deposit in the Eastern Kunlun Orogen, Western China: implications for the magmatic source, geodynamic setting and genesis. Acta Geologica Sinica - English Edition 92 (1), 106-126.

Li, R.B., Pei, X.Z., Li, Z.C., Pei, L., Liu, C.J., Chen, Y.X., Chen, G.C., Liu, Z.Q., Yang, J., 2015. Geochemistry and zircon U–Pb geochronology of granitic rocks in the Buqingshan tectonic mélange belt, northern Tibet Plateau, China and its implications for Prototethyan evolution. Journal of Asian Earth Sciences 105, 374-389.

Li, S.Z., Zhao, S.J., Liu, X., Cao, H.H., Yu, S., Li, X.Y., Somerville, I., Yu, S.Y., Suo, Y.H., 2018. Closure of the Proto-Tethys Ocean and Early Paleozoic amalgamation of microcontinental blocks in East Asia. Earth-Science Reviews 186, 37-75.

Li, W.Y., 2008. Geochronology and geochemistry of the ophiolites and island-arc-type igneous rocks in the Western Qinling orogen and the Eastern Kunlun orogen: implication for the evolution of the Tethyan Ocean. doctor. Hefei, University of Science and Technology of China. 1-174 (in Chinese with English abstract).

Liu, L., Liao, X.Y., Wang, Y.W., Wang, C., Santosh, M., Yang, M., Zhang, C.L., Chen, D.L., 2016. Early Paleozoic tectonic evolution of the North Qinling Orogenic Belt in Central China: Insights on continental deep subduction and multiphase exhumation. Earth-Science Reviews 159, 58-81.

Liu, B., Ma, C.Q., Jiang, H.A., Guo, P., Zhang, J.Y., Xiong, F.H., 2013. Early Paleozoic tectonic transition from ocean subduction to collisional orogeny in the Eastern Kunlun region: Evidence from Huxiaoqin mafic rocks. Acta Petrologica Sinica 29 (06),

2093-2106 (in Chinese with English abstract).

Liu, B., Ma, C.Q., Zhang, J.Y., Xiong, F.H., Huang, J., Jiang, H.A., 2012. Petrogenesis of Early Devonian intrusive rocks in the east part of Eastern Kunlun Orogen and implication for Early Palaeozoic orogenic processes. Actor Petrologica Sinica 28 (06), 1785-1807 (in Chinese with English abstract).

Liu, Z.Q., Pei, X.Z., Li, R.B., Li, Z.C., Chen, G.C., Chen, Y.X., Gao, J.M., Liu, C.J., Wei, F.H., Wang, X.L., Zhang, G., 2011. Early Paleozoic intermediate-acid magmatic activity in Bairiqiete area along the Buqingshan tectonic melange belt on the southern margin of East Kunlun: Constraints from zircon U-Pb dating and geochemistry. Geology in China 38 (05), 1150-1167 (in Chinese with English abstract).

Liu, Z.Q., Pei, X.Z., Li, R.B., Li, Z.C., Zhang, X.F., Liu, Z.G., Chen, G.C., Chen, Y.X., Ding, S.P., Guo, J.F., 2011. LA-ICP-MS zircon U-Pb geochronology of the two suites of ophiolites at the Buqingshan area of the A'nyemaqen Orogenic Belt in the southern margin of East Kunlun and its tectonic implication. Acta Geologica Sinica 85 (02), 185-194 (in Chinese with English abstract).

Loiselle, M.C., Wones, D.R., 1979. Characteristics and origin of anorogenic granites. Geological Society of America Abstract Progressing 11, 468.

Long, X.P., 2004. The research of zircon chronology in orogenic belts-A case study in Jinshuikou zone. master. Changchun, Jilin University. 129 (in Chinese with English abstract).

Lu, L., Wu, Z.H., Hu, D.G., Patrick, J.B., Hao, S., Zhou, C.J., 2010. Zircon U-Pb age for

rhyolite of the Maoniushan Formation and its tectonic significance in the East Kunlun Mountains. Acta Petrologica Sinica 26 (04), 1150-1158 (in Chinese with English abstract).

Lu, L., Zhang, Y.L., Wu, Z.H., Hu, D.G., 2013. Zircon U-Pb dating of Early Paleozoic granites from the East Kunlun Mountains and its geological significance. Acta Geoscientica Sinica 34 (04), 447-454 (in Chinese with English abstract).

Maniar, P.D., Piccoli, P.M., 1989. Tectonic discrimination of granitoids. Geological Society of America Bulletin 101 (5), 635-643.

Meng, F.C., Cui, M.H., Wu, X.K., Ren, Y.F., 2015. Maoniushan mafic–ultramafic rocks in the Qimantag area of Eastern Kunlun, NW China: Remnants of an early Paleozoic incipient island arc. Gondwana Research 27 (2), 745-759.

Meng, F.C., Zhang, J.X., Cui, M.H., 2013. Discovery of Early Paleozoic eclogite from the East Kunlun, Western China and its tectonic significance. Gondwana Research 23 (2), 825-836.

Middlemost, E.A.K., 1985. Magmas and magmatic rocks: an introduction to igneous petrology. Longman, London 1-266.

Miller, C.F., McDowell, S.M., Mapes, R.W., 2003. Hot and cold granites? Implications of zircon saturation temperatures and preservation of inheritance. Geology 31, 529-532.

Mo, X.X., Luo, Z.H., Deng, J.F., Yu, X.H., Liu, C.D., Chen, H.W., Yuan, W.M., Liu, Y.H., 2007. Granitoids and crustal growth in the East-Kunlun Orogenic Belt. Geological Journal of China Universities 13 (03), 403-414 (in Chinese with English abstract).

Patino Douce, A.E., 1999. What do experiments tell us about the relative contributions of crust and mantle to the origin of granitic magmas? Geological Society, London, Special Publications 168 (1), 55-75.

Pearce, J.A., Harris, N.B.W., Tindle, A.G., 1984. Trace element discrimination diagrams for the tectonic interpretation of granitic rocks. Journal of Petrology 25 (4), 956-983.

Qi, X.P., Yang, J., Fan, X.G., Cui, J.T., Cai, Z.F., Zeng, X.W., Wei, W., Qu, X.X., Zai, L.M., 2016. Age, geochemical characteristics and tectonic significance of Changshishan ophiolite in central East Kunlun tectonic mélange belt along the east section of East Kunlun Mountains. Geology in China 43 (03), 797-816 (in Chinese with English abstract).

Rapp, R.P., Watson, E.B., 1995. Dehydration melting of metabasalt at 8–32 kbar: implications for continental growth and crust-mantle recycling. Journal of Petrology 36 (4), 891-931.

Raumer, J.F.V., Stampfli, G.M., 2008. The birth of the Rheic Ocean — Early Palaeozoic subsidence patterns and subsequent tectonic plate scenarios. Tectonophysics 461 (1), 9-20.

Roche, H.D.L., Leterrier, J., Grandclaude, P., Marchal, M., 1980. A classification of volcanic and plutonic rocks using R1- R2 diagrams and major-element analyses — Its relationships with current nomenclature. Chemical Geology 29 (1–4), 183-210.

Shi, B., Zhu, Y.H., Zhong, Z.Q., Jian, K.K., 2016. Petrological, geochemical characteristics and geological significance of the caledonian peraluminous granites in Heihai region,

Eastern Kunlun. Earth Science 41 (01), 35-54 (in Chinese with English abstract).

Song, S., Bi, H., Qi, S., Yang, L., Allen, M.B., Niu, Y., Su, L., Li, W., 2018. HP–UHP metamorphic belt in the East Kunlun Orogen: final closure of the Proto-Tethys Ocean and formation of the Pan-North-China Continent. Journal of Petrology 59 (11), 2043-2060.

Song, S., Niu, Y., Su, L., Zhang, C., Zhang, L., 2014. Continental orogenesis from ocean subduction, continent collision/subduction, to orogen collapse, and orogen recycling: The example of the North Qaidam UHPM belt, NW China. Earth-Science Reviews 129, 59-84.

Sun, S.S., McDonough, W.F., 1989. Chemical and isotopic systematics of oceanic basalts: implications for mantle composition and processes. Geological Society, London, Special Publications 42 (1), 313-345.

Turner, S.P., Foden, J.D., Morrison, R.S., 1992. Derivation of some A-type magmas by fractionation of basaltic magma: an example from the Padthaway Ridge, South Australia. Lithos 28 (2), 151-179.

Wang, C., Liu, L., Xiao, P., Cao, Y., Yua, H., Meert, J.G., Liang, W., 2014. Geochemical and geochronologic constraints for Paleozoic magmatism related to the orogenic collapse in the Qimantagh-South Altyn region, northwestern China. Lithos 202-203, 1-20.

Wang, X., Wang, T., Zhang, C., 2013. Neoproterozoic, Paleozoic, and Mesozoic granitoid magmatism in the Qinling Orogen, China: Constraints on orogenic process. Journal of Asian Earth Sciences 72, 129-151.

Journal Pre-proof

Wang, G.C., Wei, Q.R., Jia, C.X., Zhang, K.X., Li, D.W., Zhu, Y.H., Xiang, S.Y., 2007. Some ideas of Precambrian geology in the East Kunlun, China. Geological Bulletin of China 26 (08), 929-937 (in Chinese with English abstract).

Watson, E.B., Wark, D.A., Thomas, J.B., 2006. Crystallization thermometers for zircon and rutile. Contributions to Mineralogy and Petrology 151 (4), 413.

Wei, B., 2015. Study on the geological characteristic and tectonic attribute of the ophiolite and island-arc-type igneous rocks, central belt of East Kunlun (eastern section). master. Xi'an, Chang'an University. 141 (in Chinese with English abstract).

Whalen, J.B., Currie, K.L., Chappell, B.W., 1987. A-type granites: geochemical characteristics, discrimination and petrogenesis. Contributions to Mineralogy and Petrology 95 (4), 407-419.

Wu, Y.B., Zheng, Y.F., 2004. Genesis of zircon and its constraints on interpretation of U-Pb age. Chinese Science Bulletin 49 (16), 1589-1604 (in Chinese with English abstract).

Wu, F.Y., Sun, D.Y., Li, H.M., Jahn, B.M., Wilde, S., 2002. A-type granites in northeastern China: age and geochemical constraints on their petrogenesis. Chemical Geology 187 (1–2), 143-173.

Xiong, F., Ma, C., Wu, L., Jiang, H., Liu, B., 2015. Geochemistry, zircon U–Pb ages and Sr–Nd–Hf isotopes of an Ordovician appinitic pluton in the East Kunlun orogen: New evidence for Proto-Tethyan subduction. Journal of Asian Earth Sciences 111, 681-697.

Xiong, L.J., 2014. Tectonic evolution and processes in the west segment of the northern Proto-Tethys tectonic domain. master. Qingdao, Ocean University of China. (in Chinese

with English abstract).

Xiong, F.H., Ma, C.Q., Zhang, J.Y., Liu, B., Jiang, H.A., 2014. Reworking of old continental lithosphere: an important crustal evolution mechanism in orogenic belts, as evidenced by Triassic I-type granitoids in the East Kunlun orogen, Northern Tibetan Plateau. Journal of the Geological Society 171 (6), 847-863.

Yang, J.H., Wu, F.Y., Chung, S.L., Wilde, S.A., Chu, M.F., 2006. A hybrid origin for the Qianshan A-type granite, northeast China: Geochemical and Sr–Nd–Hf isotopic evidence. Lithos 89 (1-2), 89-106.

Yang, J., Wang, X., Shi, D., Xu, Z., Wu, C., 2004. The Dur'ngoi ophiolite in East Kunlun, northern Qinghai-Tibet Plateau: a fragment of paleo-Tethyan oceanic crust. Geology in China 31 (03), 225-239 (in Chinese with English abstract).

Yang, J.S., Robinson, P.T., Jiang, C.F., Xu, Z.Q., 1996. Ophiolites of the Kunlun Mountains, China and their tectonic implications. Tectonophysics 258 (1), 215-231.

Yu, N., Jin, W., Ge, W.C., Long, X.P., 2005. Geochemical study on peraluminous granite from Jinshuikou in East Kunlun. Global Geology 24 (02), 123-128 (in Chinese with English abstract).

Yuan, C., Sun, M., Zhou, M.F., Zhou, H., Xiao, W.J., Li, J.L., 2002. Tectonic evolution of the West Kunlun: geochronologic and geochemical constraints from Kudi granitoids. International Geology Review 44 (7), 653-669.

Zhang, D.H., Wei, J.H., Fu, L.B., Chen, H.Y., Tan, J., Li, Y.J., Shi, W.J., Tian, N., 2013. Formation of the Jurassic Changboshan-Xieniqishan highly fractionated I-type granites,

Journal Pre-proof

northeastern China: implication for the partial melting of juvenile crust induced by asthenospheric mantle upwelling. Geological Journal 50 (2), 122-138.

Zhang, J.Y., Ma, C.Q., Xiong, F.H., Liu, B., Li, J.W., Pan, Y.M., 2014. Early Paleozoic high-Mg diorite-granodiorite in the eastern Kunlun Orogen, western China: Response to continental collision and slab break-off. Lithos 210-211, 129-146.

Zhang, L., Chen, R.X., Zheng, Y.F., Li, W.C., Hu, Z.C., Yang, Y.H., Tang, H.L., 2016. The tectonic transition from oceanic subduction to continental subduction: Zirconological constraints from two types of eclogites in the North Qaidam orogen, northern Tibet. Lithos 244, 122-139.

Zhang, C.L., Yu, H.F., Shen, J.L., Dong, Y.G., Ye, H.M., Guo, K.Y., 2004. Zircon SHRIMP age determination of the giant-crystal gabbro and basalt in Küda, West Kunlun: Dismembering of the Küda ophiolite. Geological Review 50 (06), 639-643 (in Chinese with English abstract).

Zhang, X., Yang, S., Yang, Z., 2005. An introduction to regional geology of Qinghai province, China (1:1000 0000 geological map). Geological Publishing House, Beijing 158 (in Chinese).

Zhang, Y.F., Pei, X.Z., Ding, S.P., Li, R.B., Feng, J.Y., Sun, Y., Li, Z.C., Chen, Y.X., 2010. LA-ICP-MS zircon U-Pb age of quartz diorite at the Kekesha area of Dulan County, eastern section of the East Kunlun orogenic belt, China and its significance. Geological Bulletin of China 29 (01), 79-85 (in Chinese with English abstract).

Zheng, Y., Yang, Y., Chen, B., Zhu, Y., 2016. Geochemical Characteristics and Tectonic

Significance of Gabbro from Bashikangkuole in West Part of Eastern Kunlun, China. Geoscience 30 (05), 1004-1013 (in Chinese with English abstract).

Zhou, B., Dong, Y.P., Zhang, F.F., Yang, Z., Sun, S.S., He, D.F., 2016. Geochemistry and zircon U-Pb geochronology of granitoids in the East Kunlun Orogenic Belt, northern Tibetan Plateau: origin and tectonic implications. Journal of Asian Earth Sciences 130, 265-281.

Journal Pre-proof

Journal Pre-proof

Highlights

- A Silurian-Devonian A-type granite belt is present in the East Kunlun Orogen (EKO).
- The A-type granite belt was sourced from the Ordovician–Silurian granitoids.
- The collision after the Proto-Tethys Ocean closure should be earlier than ~425 Ma.
- The post-collisional extensional event continued to ca. 385 Ma.
- The EKO should merge with Gondwana/-derived microcontinents during the Silurian.

Journal Pre-proof

Journal Pre-proof

Editors

Lithos

Dear Sir/Madam

Please find the attached manuscript entitled "Proto-Tethys magmatic evolution along northern Gondwana: Insights from Late Silurian–Middle Devonian A-type magmatism, East Kunlun Orogen, Northern Tibetan Plateau, China", by Jia-Jie Chen and coauthors, which we respectfully submit to *Lithos* for possible publication.

The East Kunlun Orogen (EKO), a microcontinent in northern Gondwana during the Paleozoic, is a giant tectono-magmatic belt located in the north of the Qinghai-Tibetan Plateau. Magmatic rocks in the EKO record two-stage orogenesis regarding the evolutions of the Proto-Tethys Ocean (Neoproterozoic–Early Paleozoic) and Paleo-Tethys Ocean (Late Paleozoic–Cenozoic) that developed along northern Gondwana and thus offer us an opportunity to detect the tectonic evolution of Tethys Ocean and northern Gondwana.

In this research, an A-type granite belt is recognized in the EKO. The origin and rock-forming tectonic setting of this belt are discussed based on our new geochronological, mineralogical, geochemical and isotopic data, and temporal-spatial distribution of regional magmatic, metamorphic and sedimentary rocks. We propose that the A-type granite belt in the EKO was formed by the partial melting of the earlier intruded Ordovician-Silurian granitoids in a post-collisional extensional setting and the Proto-Tethys Ocean should be

closed earlier than 425 Ma, which led to the EKO and adjacent terranes amalgamating into northern Gondwana or Gondwana-derived microcontinents.

The manuscript contains *ca*. 11281 words (included the reference list), 12 figures and three appendix files. The raw data (Appendix A) and a descriptive file for the related analytical method (Appendix B) are uploaded to the data repository, Mendeley Data. **The materials contained are fully the authors' work and have not been published or simultaneously submitted elsewhere in any language. The manuscript does not contain any previously unreported material that is a part of a manuscript in review or press elsewhere. No conflict of interest exists in the submission of this manuscript, and the manuscript is approved by all authors for publication.**

Thank you in advance for your time and efforts in handling our manuscript and look forward to hearing from you.

Sincerely yours,

Jun-Hao Wei (corresponding author)

Email: junhaow@163.com

Journal Pre-proof

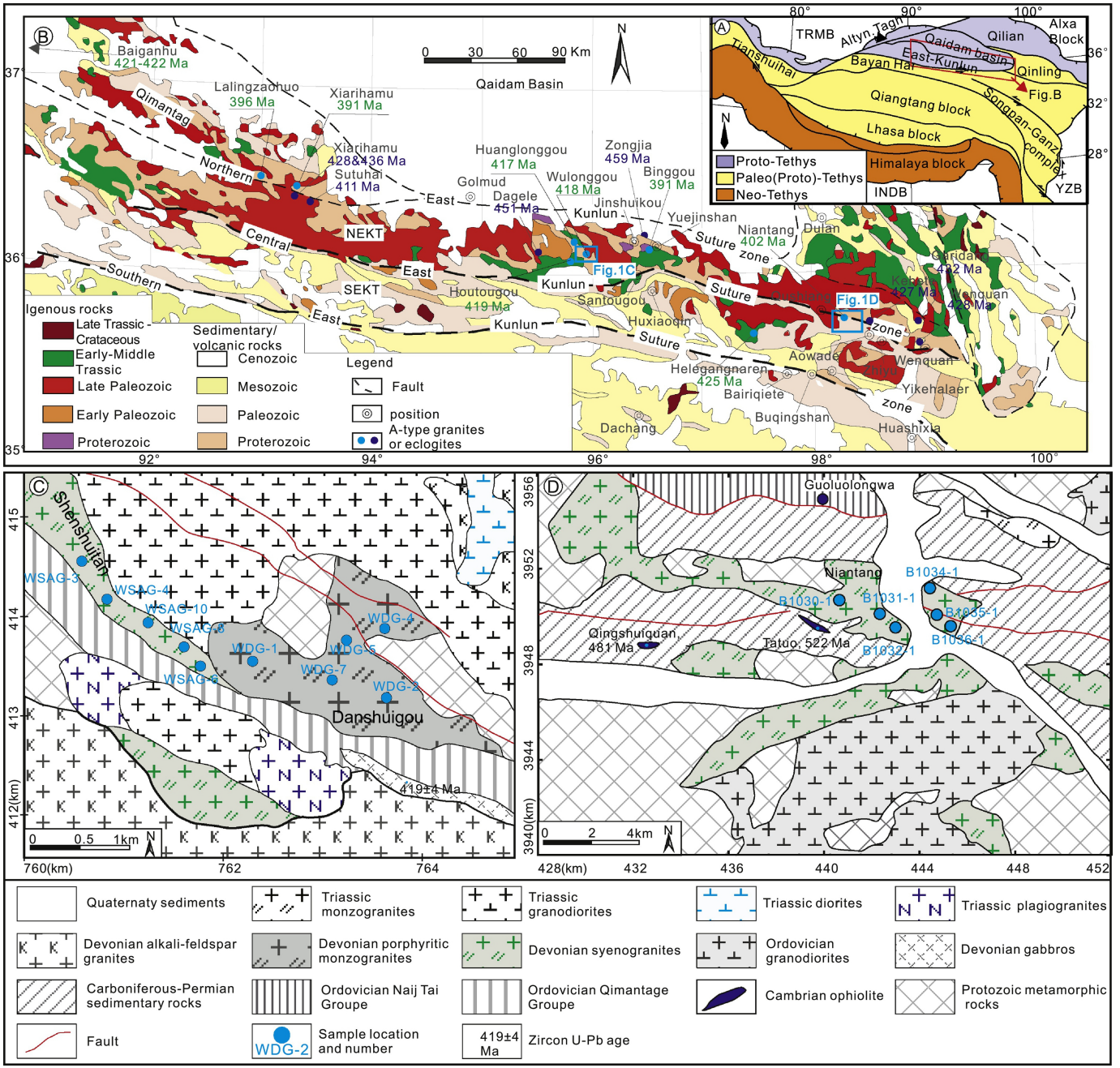
B
Baiganhu
421-422 Ma
Lalingzaohuo
396 Ma
Xiarihamu
391 Ma
Qimantag
Northern
East
Xiarihamu
428&436 Ma
Sutuhai
411 Ma
Huanglonggou
417 Ma
Golmud
Dagele
451 Ma
Wulonggou
418 Ma
Zongjia
459 Ma
Binggou
391 Ma
Jinshuikou
Kunlun
Yuejinshan
Central
NEKT
East
Southern
SEKT
East
Houtougou
419 Ma
Kunlun
Santougou
Huxiaoqin
Kunlun
Suture zone
Niantang
402 Ma
Dulan
Fig.1C
Fig.1D
Suture zone
Suture zone
Suture zone
Aowade
Helegangnaren
425 Ma
Bairiqiete
Dachang
Buqingshan
Huashixia
Yikehalaer
Wenquan
0 30 60 90 Km
N
Qaidam Basin
92°
94°
96°
98°
100°
37°
36°
35°
Igenous rocks
Late Trassic - Crataceous
Early-Middle Trassic
Late Paleozoic
Early Paleozoic
Proterozoic
Sedimentary/ volcanic rocks
Cenozoic
Mesozoic
Paleozoic
Proterozoic
Legend
Fault
position
A-type granites or eclogites
A
TRMB
Altyn-Tagh
Qaidam basin
Qilian
Alxa Block
Tianshuihai
Bayan Har
East-Kunlun
Qinling
Fig.B
Qiangtang block
Songpan-Ganzi complex
Lhasa block
Himalaya block
INDB
YZB
Proto-Tethys
Paleo(Proto)-Tethys
Neo-Tethys
80°
90°
100°
36°
32°
28°
C
Shenshuitan
WSAG-3
WSAG-4
WSAG-10
WSAG-8
WSAG-9
WDG-1
WDG-4
WDG-5
WDG-7
WDG-2
Dapshuigou
419±4 Ma
0 0.5 1km
N
415
414
413
412(km)
760(km)
762
764
D
Guoluolongwa
Niantang
B1034-1
B1031-1
B1030-1
B1035-1
B1036-1
B1032-1
Qingshuiquan,
481 Ma
Tatuo: 522 Ma
0 2 4km
N
3956
3952
3948
3944
3940(km)
428(km)
432
436
440
444
448
452
Quaternaty sediments
Triassic monzogranites
Triassic granodiorites
Triassic diorites
Triassic plagiogranites
Devonian alkali-feldspar granites
Devonian porphyritic monzogranites
Devonian syenogranites
Ordovician granodiorites
Devonian gabbros
Carboniferous-Permian sedimentary rocks
Ordovician Naij Tai Groupe
Ordovician Qimantage Groupe
Cambrian ophiolite
Protozoic metamorphic rocks
Fault
Sample location and number
WDG-2
419±4 Ma
Zircon U-Pb age

Figure 1

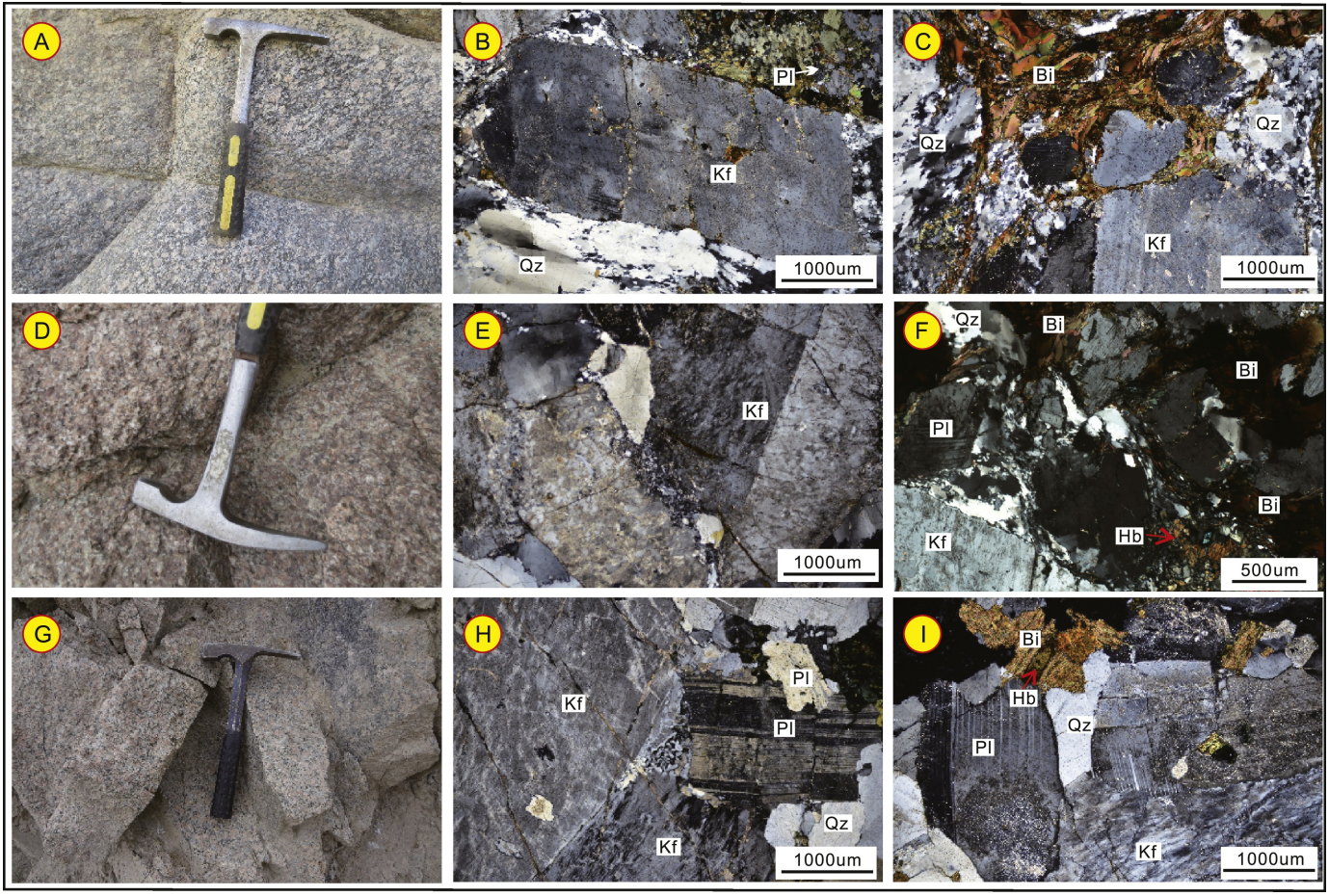
A
B
Pl
Kf
Qz
1000um
C
Bi
Qz
Qz
Kf
1000um
D
E
Kf
1000um
F
Qz
Bi
Bi
Pl
Bi
Kf
Hb
500um
G
H
Pl
Kf
Pl
Qz
Kf
1000um
I
Bi
Hb
Qz
Pl
Kf
1000um

Figure 2

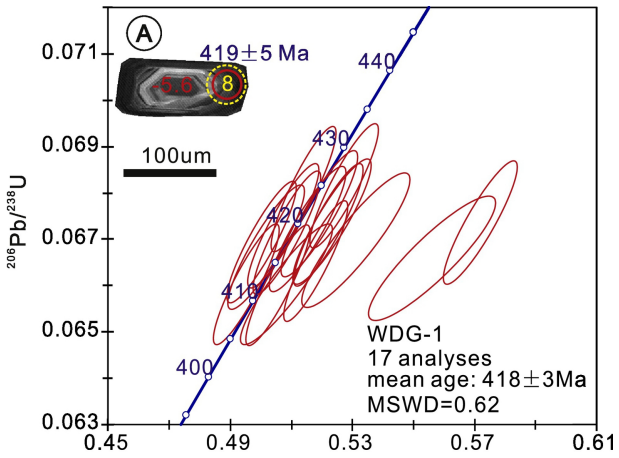
A
419±5 Ma
-5.6
8
100um
440
430
420
410
400
WDG-1
17 analyses
mean age: 418±3Ma
MSWD=0.62
$^{206}Pb/^{238}U$

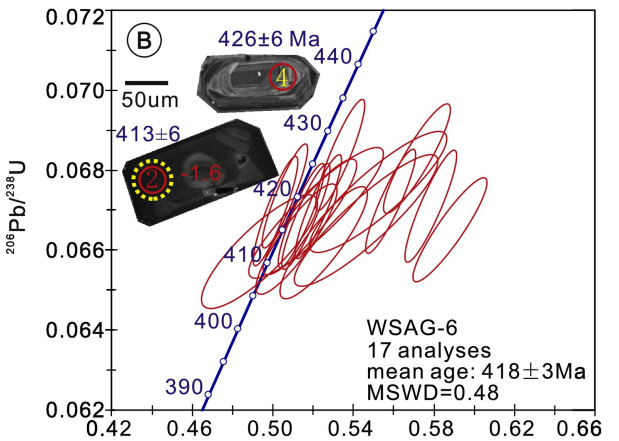
B
426±6 Ma
4
50um
413±6
2
-1.6
440
430
420
410
400
390
WSAG-6
17 analyses
mean age: 418±3Ma
MSWD=0.48
$^{206}Pb/^{238}U$

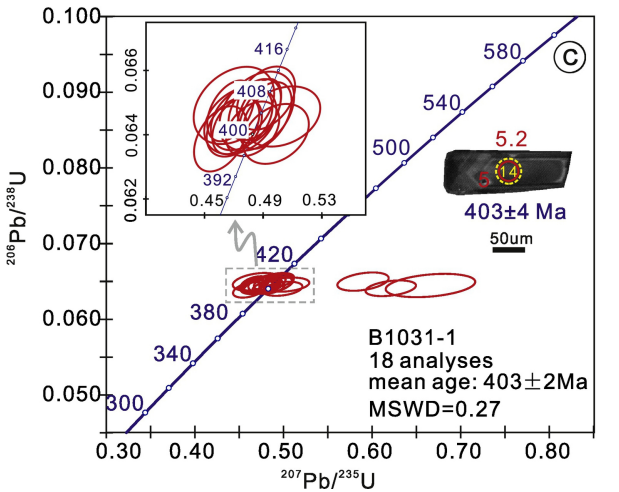
C
416
408
400
392
580
540
500
5.2
5.1
14
403±4 Ma
50um
420
380
340
300
B1031-1
18 analyses
mean age: 403±2Ma
MSWD=0.27
$^{206}Pb/^{238}U$
$^{207}Pb/^{235}U$

Figure 3

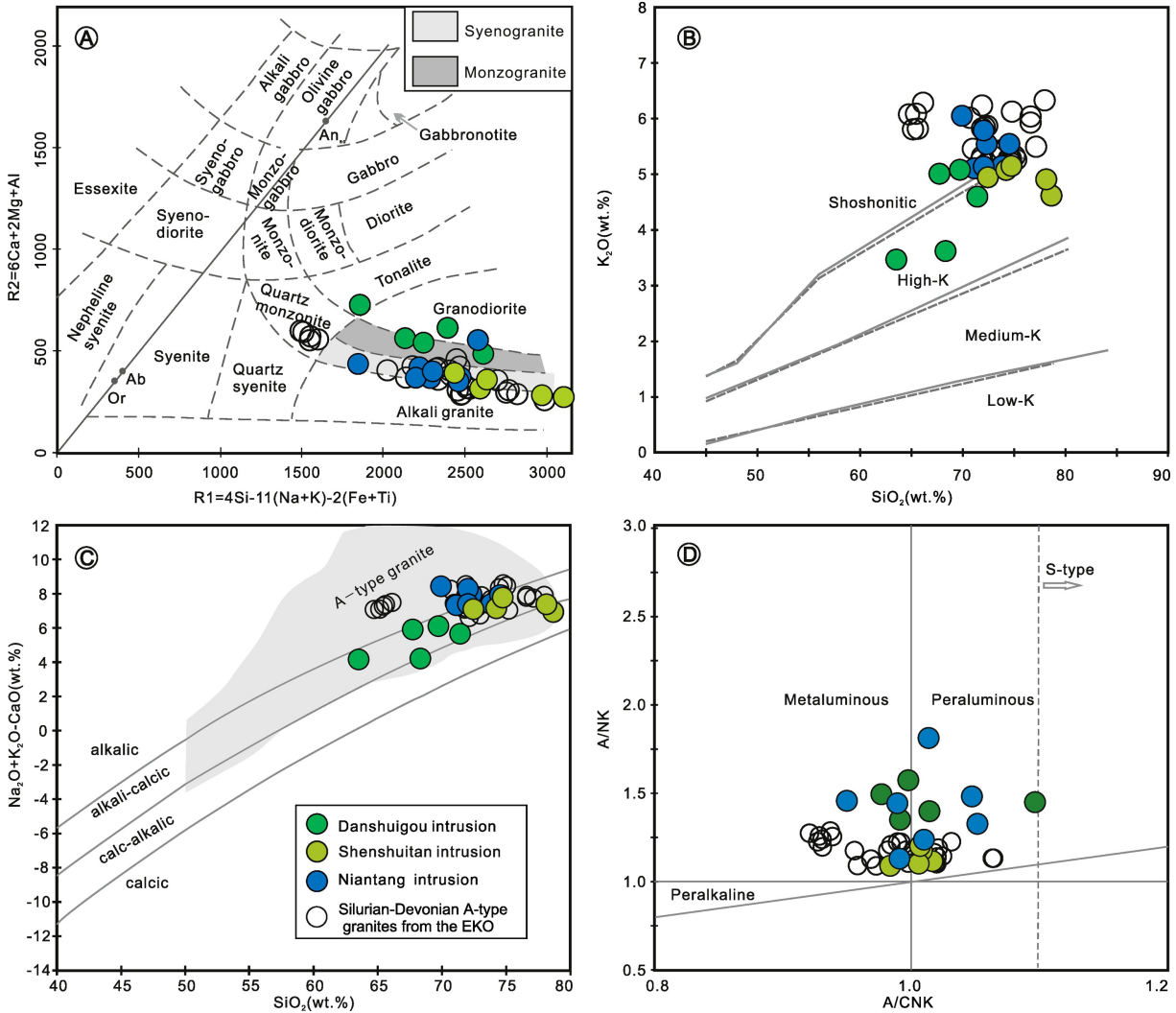
Ⓐ
Syenogranite
Monzogranite
Alkali gabbro
Olivine gabbro
An
Gabbronotite
Syeno-gabbro
Monzo-gabbro
Gabbro
Essexite
Syeno-diorite
Monzo-nite
Monzo-diorite
Diorite
Tonalite
Quartz monzonite
Granodiorite
Nepheline syenite
Syenite
Quartz syenite
Ab
Or
Alkali granite
R2=6Ca+2Mg+Al
R1=4Si-11(Na+K)-2(Fe+Ti)
Ⓑ
Shoshonitic
High-K
Medium-K
Low-K
K2O(wt.%)
SiO2(wt.%)
Ⓒ
A−type granite
alkalic
alkali-calcic
calc-alkalic
calcic
Danshuigou intrusion
Shenshuitan intrusion
Niantang intrusion
Silurian-Devonian A-type granites from the EKO
Na2O+K2O-CaO(wt.%)
SiO2(wt.%)
Ⓓ
S-type
Metaluminous
Peraluminous
Peralkaline
A/NK
A/CNK

Figure 4

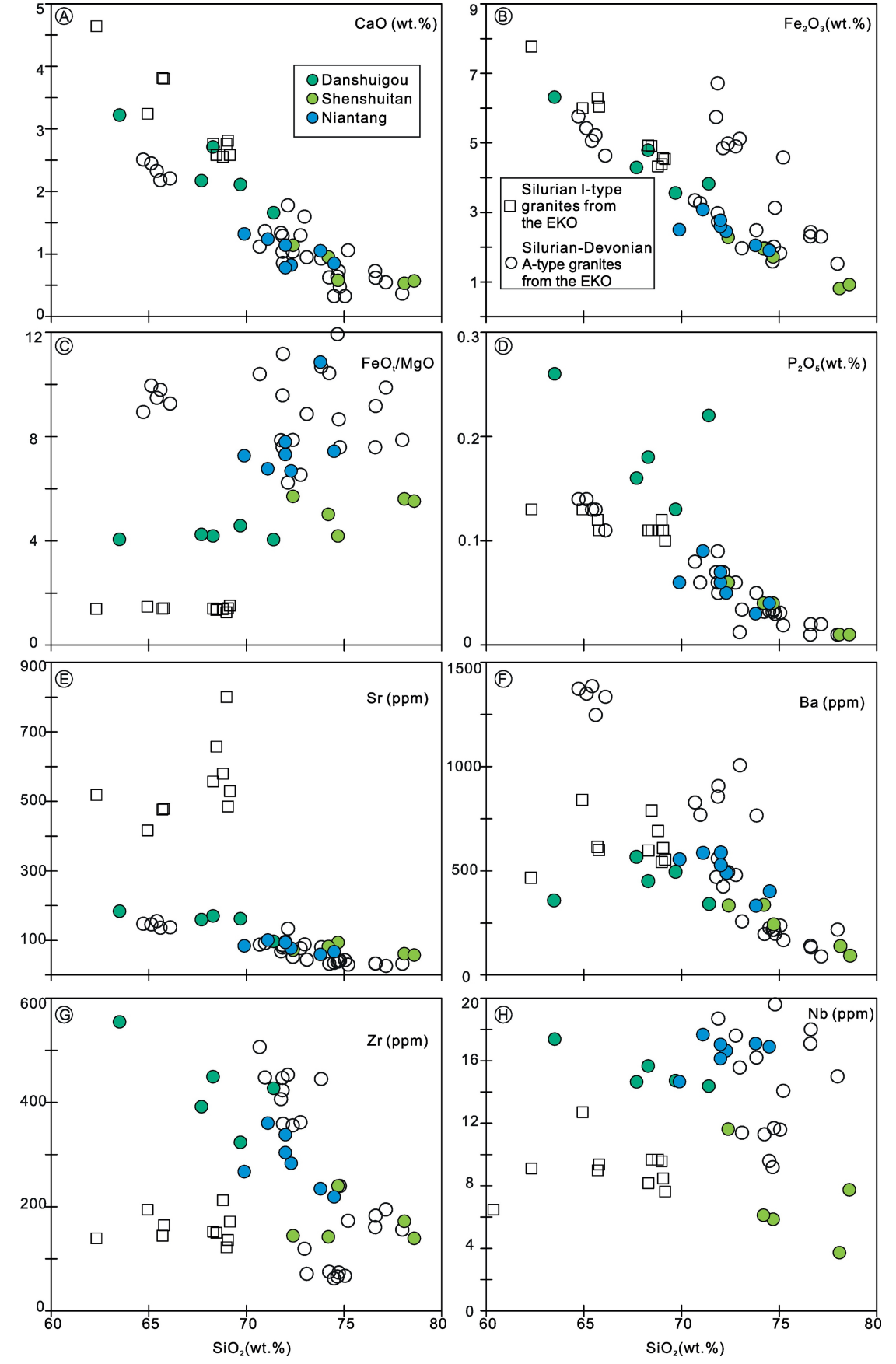
Ⓐ
CaO (wt.%)
Danshuigou
Shenshuitan
Niantang
Ⓑ
Fe2O3(wt.%)
Silurian I-type granites from the EKO
Silurian-Devonian A-type granites from the EKO
Ⓒ
FeOt/MgO
Ⓓ
P2O5(wt.%)
Ⓔ
Sr (ppm)
Ⓕ
Ba (ppm)
Ⓖ
Zr (ppm)
Ⓗ
Nb (ppm)
SiO2(wt.%)
SiO2(wt.%)

Figure 5

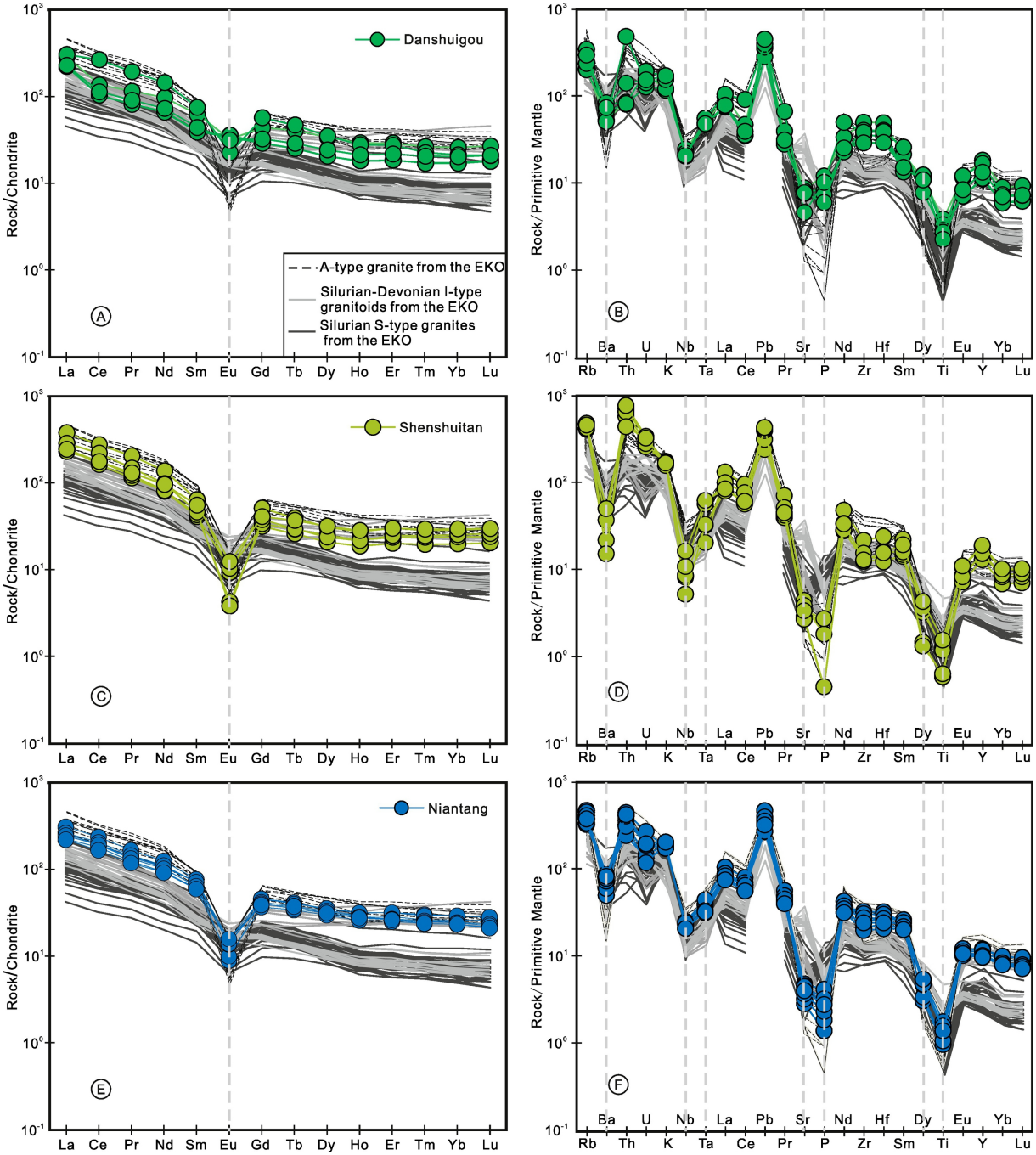
Danshuigou
A-type granite from the EKO
Silurian-Devonian I-type granitoids from the EKO
Silurian S-type granites from the EKO
Shenshuitan
Niantang
Rock/Chondrite
Rock/Primitive Mantle
A
B
C
D
E
F
La Ce Pr Nd Sm Eu Gd Tb Dy Ho Er Tm Yb Lu
Rb Ba Th U K Nb Ta La Ce Pb Pr Sr P Nd Zr Hf Sm Ti Dy Y Eu Yb Lu

Figure 6

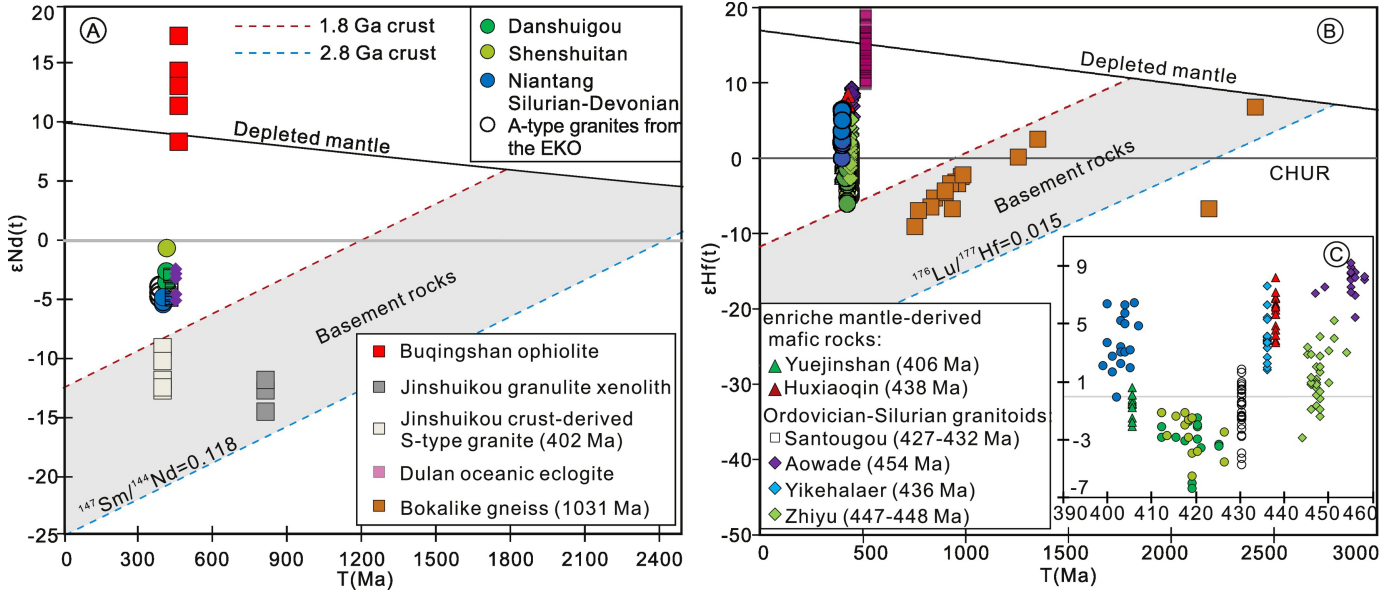
A
1.8 Ga crust
2.8 Ga crust
Depleted mantle
Basement rocks
Danshuigou
Shenshuitan
Niantang
Silurian-Devonian
A-type granites from
the EKO
Buqingshan ophiolite
Jinshuikou granulite xenolith
Jinshuikou crust-derived
S-type granite (402 Ma)
Dulan oceanic eclogite
Bokalike gneiss (1031 Ma)
147Sm/144Nd=0.118
εNd(t)
T(Ma)
B
Depleted mantle
Basement rocks
CHUR
176Lu/177Hf=0.015
enriche mantle-derived
mafic rocks:
Yuejinshan (406 Ma)
Huxiaoqin (438 Ma)
Ordovician-Silurian granitoids:
Santougou (427-432 Ma)
Aowade (454 Ma)
Yikehalaer (436 Ma)
Zhiyu (447-448 Ma)
εHf(t)
T(Ma)
C

Figure 7

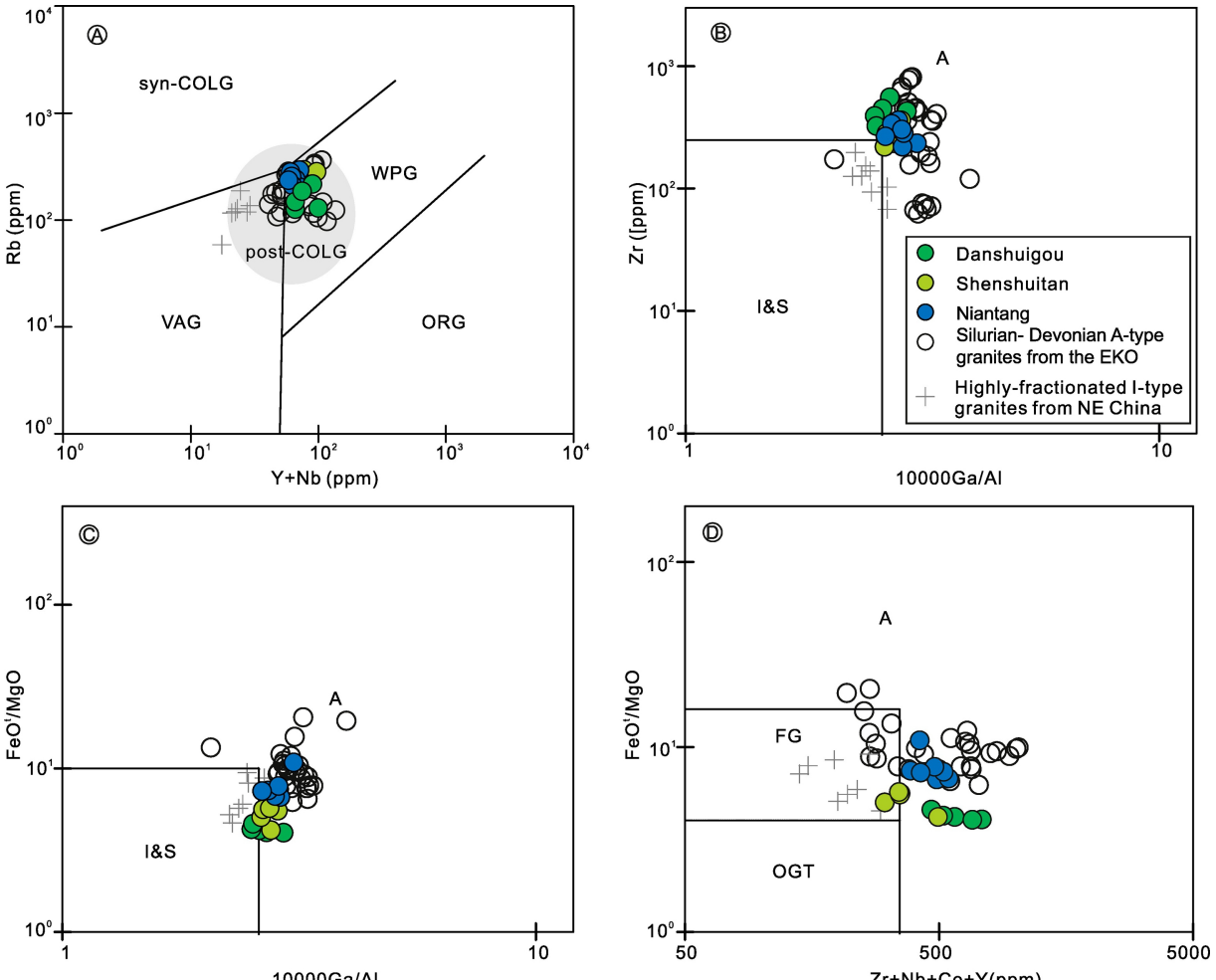
Ⓐ
syn-COLG
WPG
post-COLG
VAG
ORG
Rb (ppm)
Y+Nb (ppm)
Ⓑ
A
I&S
Zr ([ppm)
10000Ga/Al
Danshuigou
Shenshuitan
Niantang
Silurian- Devonian A-type granites from the EKO
Highly-fractionated I-type granites from NE China
Ⓒ
A
I&S
FeO'/MgO
10000Ga/Al
Ⓓ
A
FG
OGT
FeO'/MgO
Zr+Nb+Ce+Y(ppm)

Figure 8

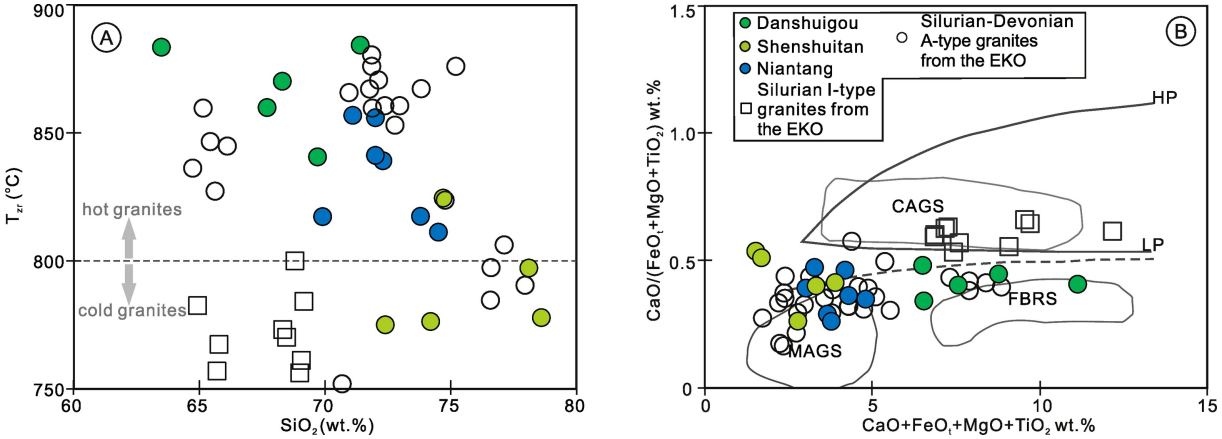
A
900
850
800
750
60
65
70
75
80
T_{zr} (°C)
SiO_2(wt.%)
hot granites
cold granites
B
Danshuigou
Shenshuitan
Niantang
Silurian I-type granites from the EKO
Silurian-Devonian A-type granites from the EKO
HP
LP
CAGS
FBRS
MAGS
1.5
1.0
0.5
0
5
10
15
$CaO/(FeO_t+MgO+TiO_2)$ wt.%
$CaO+FeO_t+MgO+TiO_2$ wt.%

Figure 9

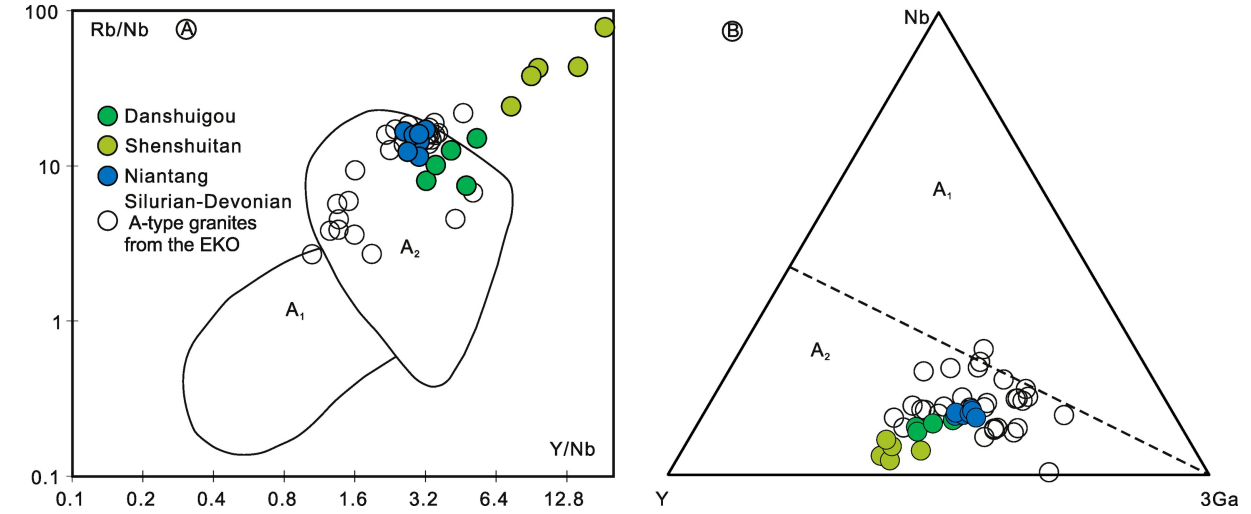
Rb/Nb
Ⓐ
Danshuigou
Shenshuitan
Niantang
Silurian-Devonian
A-type granites
from the EKO
A1
A2
Y/Nb
100
10
1
0.1
0.1
0.2
0.4
0.8
1.6
3.2
6.4
12.8
Ⓑ
Nb
A1
A2
Y
3Ga

Figure 10

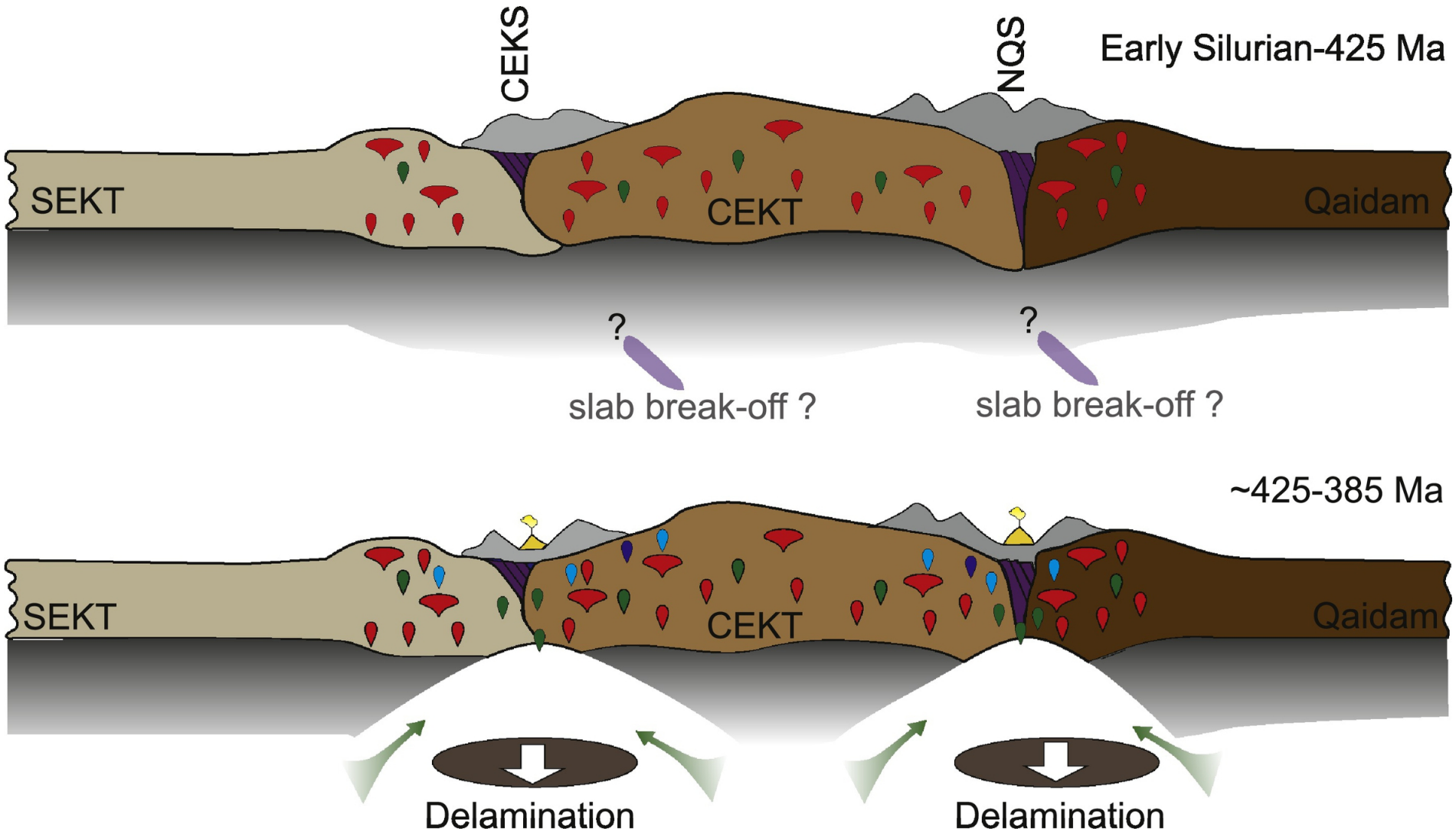
CEKS
NQS
Early Silurian-425 Ma
SEKT
CEKT
Qaidam
?
?
slab break-off ?
slab break-off ?
~425-385 Ma
SEKT
CEKT
Qaidam
Delamination
Delamination

Figure 11

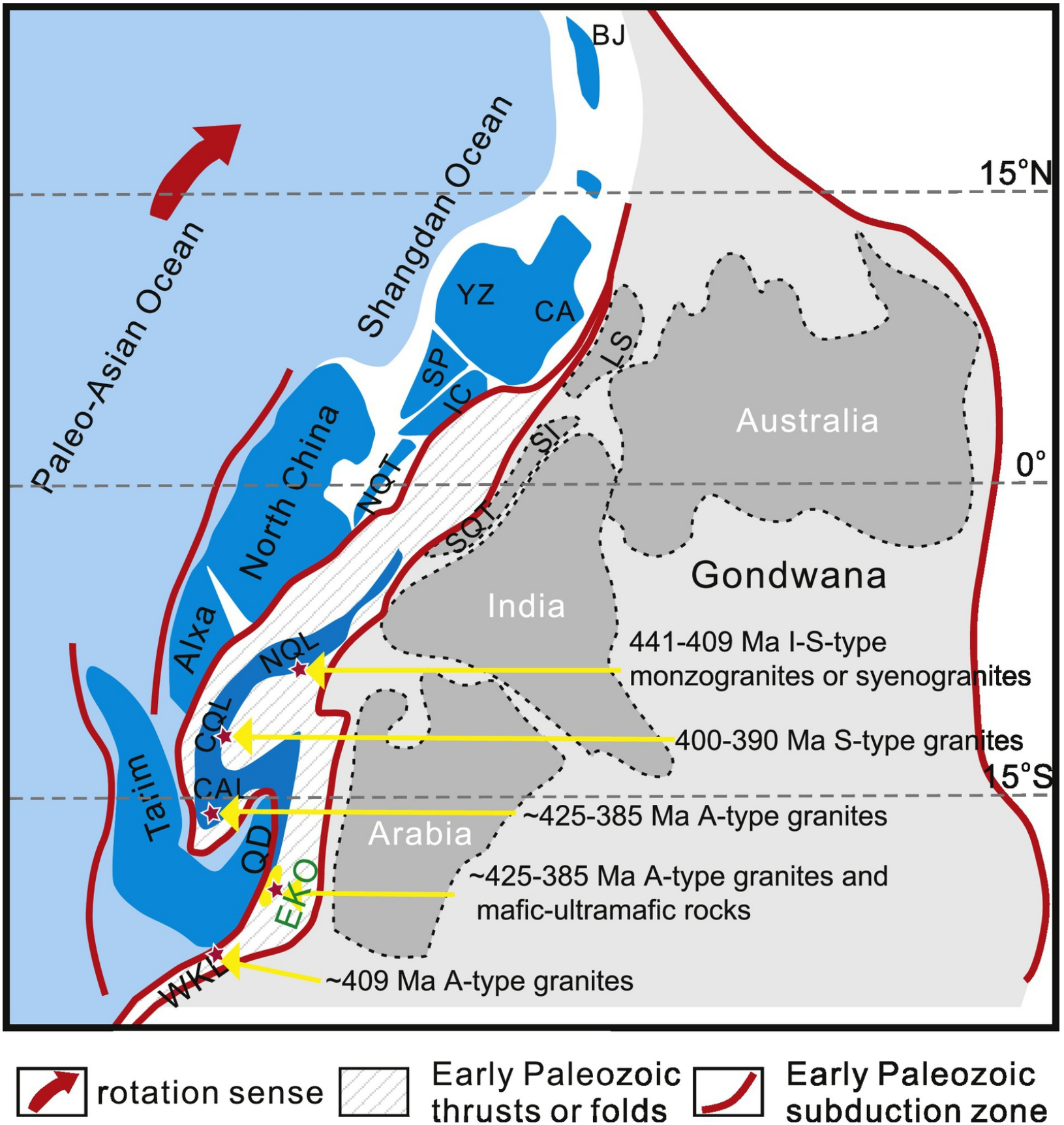
BJ
Shangdan Ocean
Paleo-Asian Ocean
15°N
YZ
CA
SP
IC
LS
Australia
0°
NQT
SI
SQT
North China
Gondwana
India
Alxa
NQL
441-409 Ma I-S-type
monzogranites or syenogranites
CQL
400-390 Ma S-type granites
15°S
Tarim
CAL
~425-385 Ma A-type granites
Arabia
QD
EKO
~425-385 Ma A-type granites and
mafic-ultramafic rocks
WKL
~409 Ma A-type granites
rotation sense
Early Paleozoic
thrusts or folds
Early Paleozoic
subduction zone

Figure 12